

High-Temperature Friction and Wear Studies of Nimonic 80A and Nimonic 90 Against Nimonic 75 Under Dry Sliding Conditions

G. Khajuria¹ · M. F. Wani¹

Received: 21 January 2017 / Accepted: 16 June 2017
© Springer Science+Business Media, LLC 2017

Abstract The present research focuses on dry sliding friction and wear behaviour of Nimonic 80A and Nimonic 90 against Nimonic 75 at high temperature up to 1023 K. The influence of temperature, sliding distance and normal load on friction and wear behaviour of Nimonic 80A and Nimonic 90 against Nimonic 75 was studied using pin (Nimonic 75)-on-disc (Nimonic 80A and Nimonic 90). Lower wear and lower friction of superalloys was observed at high temperatures, as compared to room temperature. Surface morphological and surface analytical studies of fresh and worn surfaces were carried out using optical microscopy, 3D profilometer, scanning electron microscope, energy-dispersive X-ray spectroscopy and Raman spectroscopy to understand the friction and wear behaviour. The mechanism of the formation of microscale glaze layer is also discussed.

Keywords Nickel superalloy · High temperature · Friction · Wear · Surface roughness · Glaze layer

1 Introduction

Nickel-based superalloys possess excellent mechanical and anti-corrosion properties at evaluated temperatures [1, 2]. These alloys are now used for design and fabrication of machine elements subjected to high temperature

in aeronautical, marine, nuclear, petrochemical and automobile industries. The Nimonic series of nickel-based superalloys mainly consist of nickel, chromium and aluminium and are known for their oxidation resistance, corrosion resistance, high creep strength, thermal stability, high hardness and high wear resistance at high temperatures [3–6]. Nimonic 80A (N 80A) is nickel–chromium superalloy, strengthened by additions of titanium, aluminium and carbon, developed for application at temperatures up to 1088 K. Nimonic 90 (N 90) is a creep-resistant alloy, developed for application at temperatures up to 1193 K. N 90 is developed by replacing about 20% of nickel with cobalt. The cobalt addition in N 90 raises the solubility temperature of γ' , and also it decreases the amount of carbides present by increasing the solubility of carbon in matrix. It has good ductility and is typically used in high-temperature springs [4, 7, 8]. Nimonic 75 (N 75) is a uniform solid solution of Ni–20Cr with intra-granularly occurring primary carbides of general form MC as well as chromium-rich grain boundary carbides of type $M_{23}C_6$. It is now mostly used for sheet applications calling for oxidation and scaling resistance coupled with medium strength at high operating temperatures [4, 9, 10]. Exhaust valves internal combustion engines suffer severe wear due to high temperature and pressure of exhaust gases. Wear of exhaust valves and seat inserts, effect the performance and life of engine adversely [11, 12]. In order to increase efficiency and life of engine, researchers are continuously working to minimize wear of valve seat and seat [13–16]. In this endeavour, wear-resistant surfaces of uncoated and coated materials, especially for high-temperature conditions, have been developed for valve and seat inserts through tribological research studies conducted worldwide.

✉ M. F. Wani
mfwani@nitsri.net

¹ Tribology Laboratory, Mechanical Engineering Department, National Institute of Technology Srinagar, Hazratbal, Srinagar, Kashmir 190006, India

Tribological studies of Incoloy MA956 and N 80A against Stellite 6 were conducted at room temperature to high temperature (1023 K), under dry sliding conditions [16, 17]. In these research studies, it has been observed that at low sliding speed of 0.314 ms^{-1} , mild oxidational wear occurred at all temperatures due to oxidation of wear debris and transfer of material took place from counterface (Stellite 6) to Incoloy MA956 and N 80A. It has also been observed that at room temperature to 723 K, the debris mainly took the form of loose particles with limited compaction, whereas between 783 and 1023 K the debris were compacted and sintered together to form a Co–Cr-based wear-protective ‘glaze’ layer. However, at high sliding speed of 0.905 ms^{-1} , mild oxidational wear occurred at room temperature to 723 K and no glazed layer was formed at the interface. At higher temperature from 723 to 903 K, no oxide formation was observed at the interface and direct metal-to-metal contact persisted between Incoloy MA956 and N 80A against Stellite 6. This culminated into severe wear of Incoloy MA956 and N 80A. At highest temperature from 963 to 1023 K, ‘glaze’ layer was formed at the interface due to oxidation of wear debris and no severe wear was observed. Therefore, the formation of glazed layer helped in reducing the wear of alloys to a large extent. Friction and wear studies on Inconel 617 against Stellite 6 alloys at 1023 K with a constant sliding speed of 0.025 ms^{-1} , under 5 N applied load, were conducted, using high-temperature ball-on-disc sliding wear tester [18]. In this research study, it has been observed that coefficient of friction (μ) exhibit running in behaviour and also decreased with sliding distance. Lower wear of Inconel 617 and Stellite 6 alloys were observed at higher temperature of 1023 K, in comparison with wear observed at room temperature. The adhesive and the relatively more plastic Cr_2O_3 surface layer formed between the interface of Inconel 617 and Stellite 6 alloys sustains the sliding wear action without spalling and is claimed to be responsible for the improved wear resistance of these alloys at 1023 K.

Various researchers have observed the transition from severe wear (metal-to-metal contact and high wear losses) to mild wear (oxide preventing metal-to-metal contact and keeping wear to low levels) occurred under variable conditions of load, speed and temperature [19–21]. In these research studies, it has been observed that mild wear occurs under all conditions of load, speed and temperature; nevertheless, it is time dependent. The reduction in wear has been attributed to the formations of glazed layer at the interface. Tribological studies to understand mechanism of protective glazed layer formation and its role in controlling friction and wear at high temperatures between various tribo-pairs were conducted [22–28]. It was observed that at elevated temperature wear behaviour of metallic materials is influenced by

different types of surface layer formation. In this research study, it has also been observed that formation of oxide layer depends upon transfer of material at the interface, which leads to formation of mixed metal layer (MML). The mechanism of glazed layer formation described by [13–19, 22, 23] suggests that the protective glaze layer formation takes place due to the joint action of debris generation, oxidation, elemental transfer and debris sintering between contacting surfaces.

It is evident from above literature review that various investigations have been conducted to study and improve tribological behaviour of nickel-based superalloys for high-temperature applications [13–19, 22, 23]. However, no research study has been reported in the literature on friction and wear of N 80A and N 90 superalloys against N 75 at low and high temperatures. In order to understand friction and wear behaviour of N 80A and N 90 superalloys under high-temperature sliding conditions, it is inevitable to conduct detailed high-temperature sliding wear studies on N 80A and N 90 superalloys. In the present study, the tribological behaviour of N 80A and N 90 against N 75 has been conducted under dry sliding conditions to study the influence of temperature, sliding distance and normal load on friction and wear characteristics of these two nickel superalloy using rotary arrangement high-precision tribometer and to examine the microscale or nanoscale structures of glaze layer formation and its responsible mechanisms at high temperatures using optical microscope, 3D profilometer, scanning electron microscope (SEM), energy-dispersive X-ray spectroscopy (EDS) and Raman spectroscopy.

2 Experimental Details

2.1 Materials

Nickel-based superalloys: N 80A, N 90 and N 75, were procured from commercially available reliable sources, in the form of discs 30 mm in diameter and 8 mm in thickness. Chemical composition, physical properties and mechanical properties of alloys are given in Tables 1 and 2. The surface preparation procedure of the samples consisted of grinding disc surfaces and final polishing. Disc samples are finished by SiC papers with different

Table 1 Nominal composition of alloys (wt %)

| Element | Ni | Cr | Ti | Al | Fe | C | Ta | Co |
|---------|-------|-------|------|------|------|------|------|-------|
| N 80A | 73.71 | 19.94 | 2.40 | 1.42 | 2.11 | 0.11 | 0.30 | – |
| N 90 | 50.69 | 25.80 | 3.47 | 4.38 | – | 1.49 | – | 14.17 |
| N 75 | 75.38 | 18.21 | 2.13 | 1.94 | 0.54 | 0.81 | 0.98 | – |

Table 2 Physical and mechanical properties of alloys

| Elements | Density (g/cm ³) | Melting range (°C) | Tensile strength (annealed) [MPa] | Elongation at break (%) | Modulus of elasticity (GPa) |
|----------|------------------------------|--------------------|-----------------------------------|-------------------------|-----------------------------|
| N 80A | 8.19 | 1320–1365 | 802 | 30 | 222 |
| N 90 | 8.18 | 1310–1370 | 865 | 33 | 213 |
| N 75 | 8.37 | 1340–1380 | 750 | 42 | 206 |

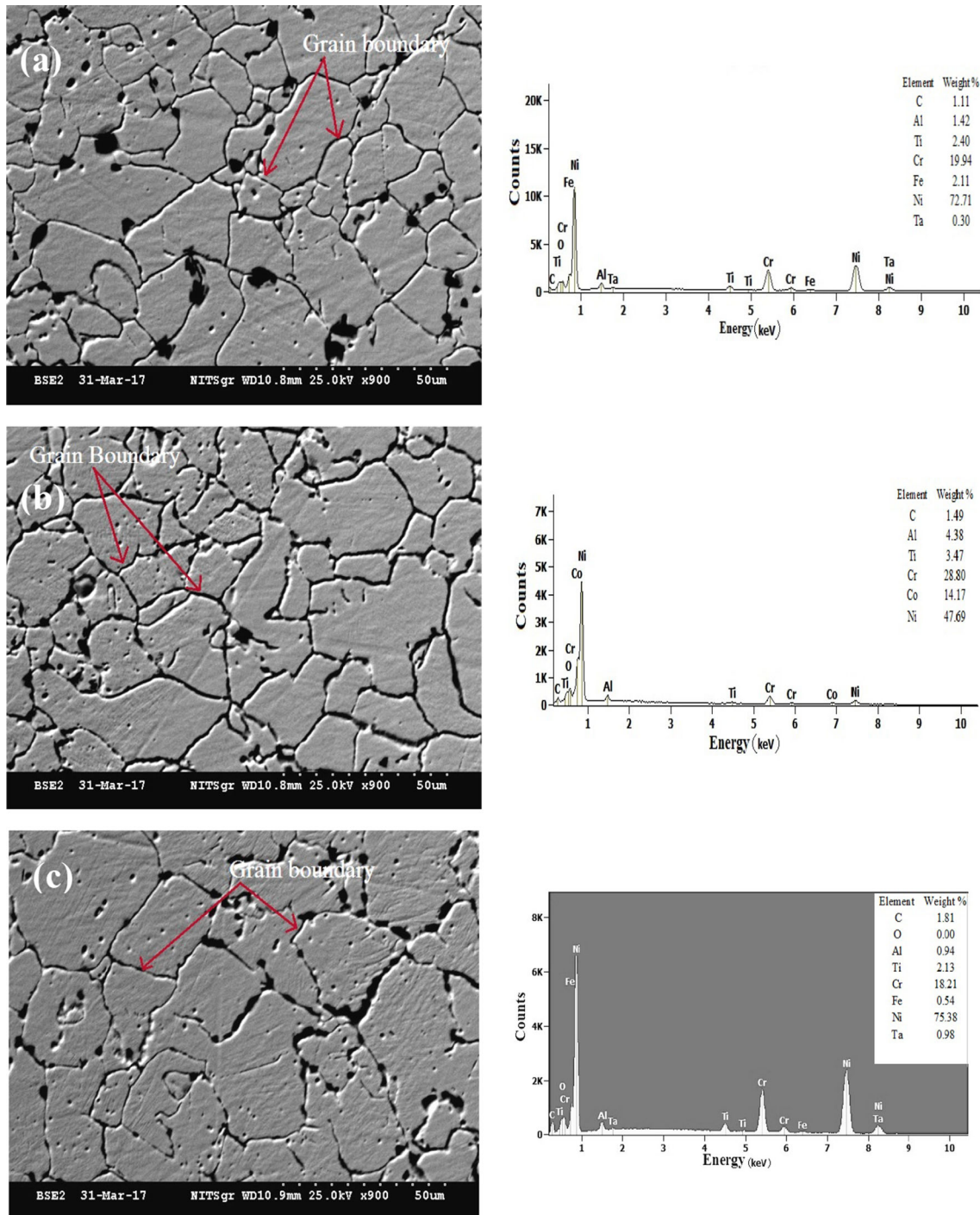


Fig. 1 SEM micrographs and EDS spectra of a N 80A, b N 90 and c N 75

Fig. 2 **a** Schematic representation of high-precision tribological test rig. 1 Load actuator, 2 spring, 3 pin holder, 4 load sensor, 5 closed heating chamber, 6 X–Y platform, **b** pin-on-disc arrangement of materials in closed heating chamber of test rig and **c** inside view of closed heating chamber at 1023 K. 7 Heating coils, 8 sample's holder, 9 sample, 10 wear scar

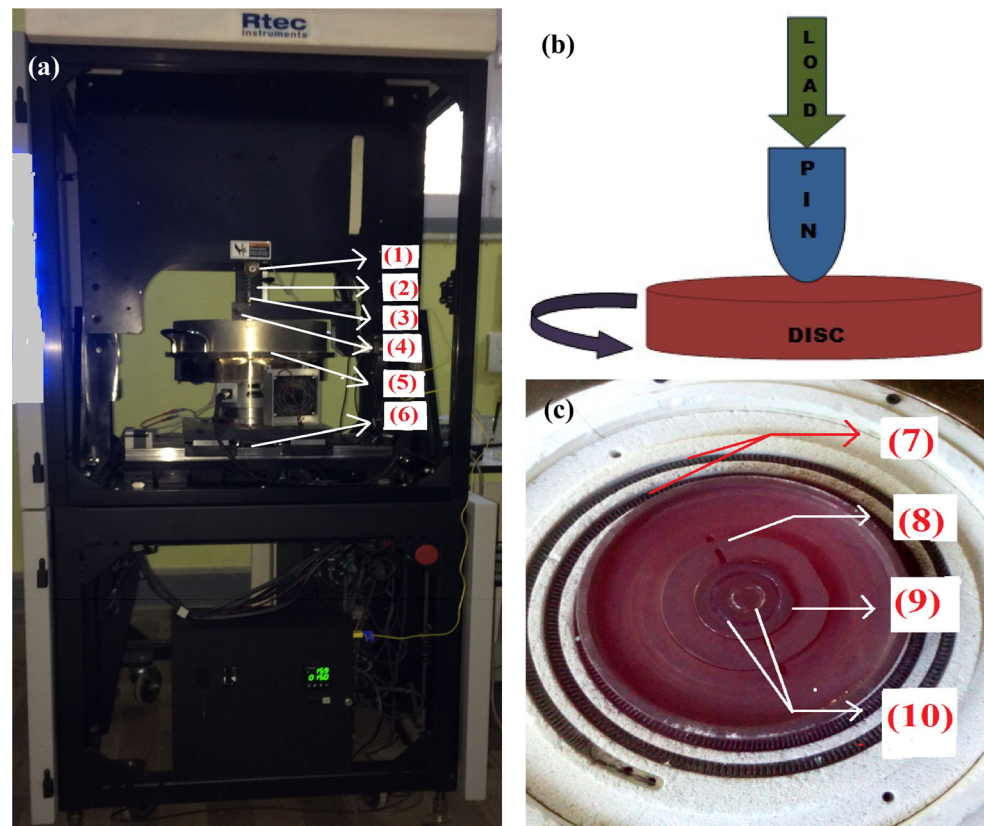


Table 3 Test parameters for conducting dry sliding wear on N 80A and N 90

| S. no. | Parameters | Magnitude of varied parameter (fixed parameters during test) | |
|--------|------------------------------|---|-----------|
| 1. | Sliding temperature (K) | RT, 483, 663, 843, 1023 (7 N, 0.314 ms ⁻¹) | |
| 2. | Sliding distance (m) | 90, 180, 270, 360, 450, 540 (1023 K, 0.314 ms ⁻¹) | |
| 3. | Load (N) | 10, 20, 30, 40 (1023 K, 0.314 ms ⁻¹) | |
| 4. | Sliding path diameter | 25 mm | |
| 5. | Pin diameter | 5.42 mm | |
| 6. | <i>Pin geometry</i> | | |
| | Length of pin | 11.56 mm | |
| | Length of pin tip | 3.46 mm | |
| | Diameter of pin tip | 2.47 mm | |
| 7. | <i>Contact area diameter</i> | N 80A/N 75 | N 90/N 75 |
| | At the start | 0.076 mm | 0.077 mm |
| | At the end | 2.47 mm | 2.47 mm |
| 8. | <i>Specific pressure</i> | | |
| | At the start | 2.31 GPa | 2.28 GPa |
| | At the end | 1.46 MPa | 1.46 MPa |
| 9. | Rotation frequency | 3.99–4 Hz | |

grit sizes, P 200, P 400, P 600, P 800, P 1200, P 1600 and P 2000, respectively, on the polishing machine at constant rpm of 1200. For ultrafine polishing of these samples, diamond pastes of 6, 4, 1 and 0.25 μm were

used. Further, these samples were cleaned in the acetone solution which was held in digital ultrasonic cleaner for 15 min. Then, the samples were dried in oven for 10 min at constant temp of 323 K. The surfaces of samples of N

Fig. 3 Average Vickers hardness of Nimonic 80A versus indentation load at different dwell times

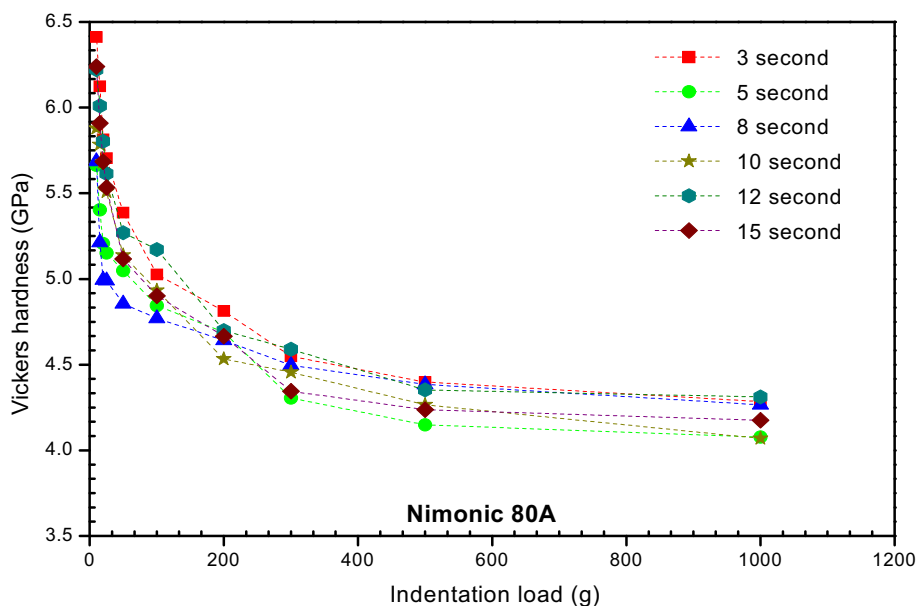
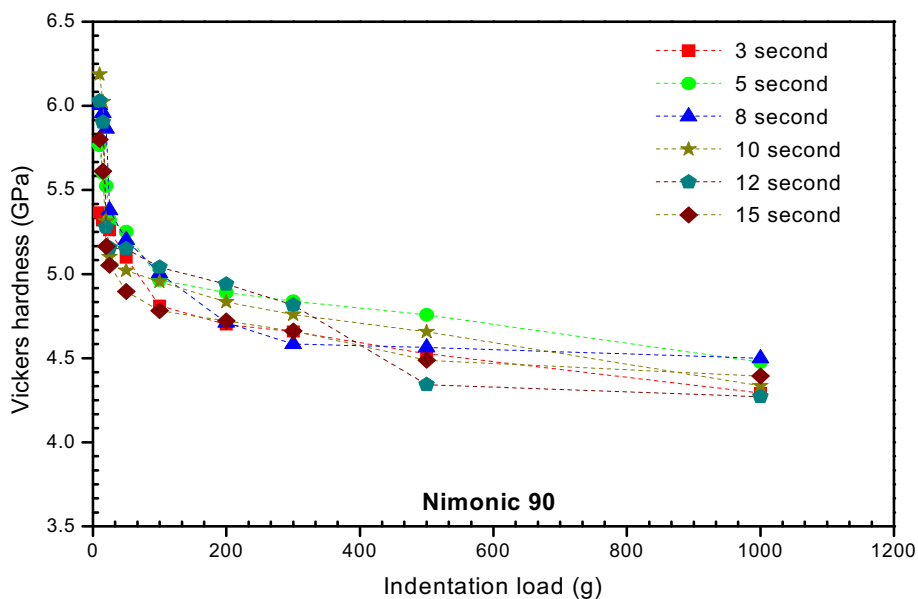


Fig. 4 Average Vickers hardness of Nimonic 90 versus indentation load at different dwell times



80A and N 90 and counterface of N 75 superalloy were mirror polished, and the average roughness (Ra) values attained were 22, 20 and 25 nm for N 80A, N 90 and N 75, respectively. Scanning electron microscopy (SEM) and energy-dispersive X-ray spectroscopy (EDS) studies were carried out to study microstructure of N 80A, N 90 and N 75 surfaces and also to carry out elemental analysis of these samples. SEM and EDS studies were carried out on SEM 3600 N (Hitachi, Jp), equipped with EDS. Typical results of SEM with EDS are shown in Fig. 1. It is evident from Fig. 1 that the surfaces of these samples contain uniform grain structure.

2.2 Microhardness Test

The Vickers microhardness (HV) was evaluated to determine the surface hardness of N 80A and N 90 superalloys by using a microhardness tester. The tests were carried out at a different indentation load ranging from 10 to 1000 g and at dwell time of 3–15 s. Each test was conducted minimum five times for better repeatability. The relationship between *P* (applied load) and *A* (area) with hardness (*H*) is represented in Eq. (1) [29] as:

$$H = \frac{P}{A} = \beta \frac{P}{d^2} \tag{1}$$

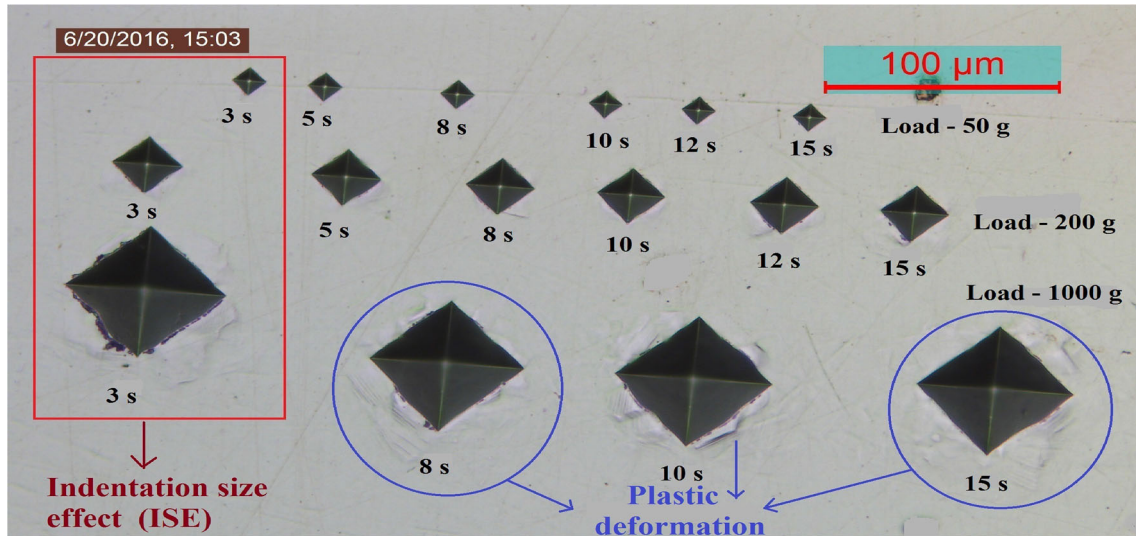


Fig. 5 Optical micrograph of indent impression at different indentation loads and dwell times

Fig. 6 Friction coefficient of Nimonic 80A and Nimonic 90 versus temperature

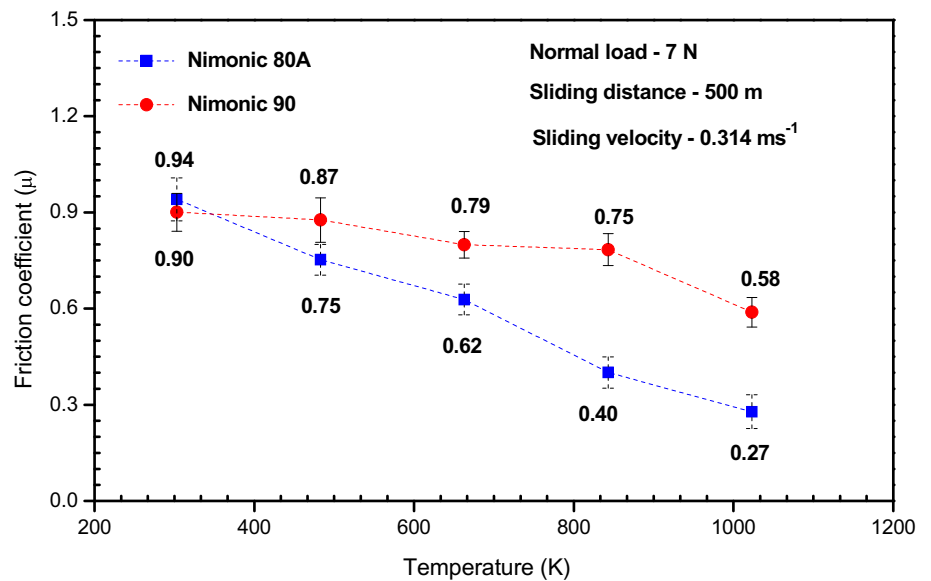


Table 4 Friction coefficient and wear volume loss of samples and counterface versus temperature

| Temperature (K) | N 80A against N 75 | | | N 90 against N 75 | | |
|-----------------|--------------------------------|---|--|--------------------------------|---|--|
| | Friction coefficient (μ) | Disc wear volume loss (mm^3) | Pin wear volume loss (mm^3) | Friction coefficient (μ) | Disc wear volume loss (mm^3) | Pin wear volume loss (mm^3) |
| RT | 0.94 | 0.99 | 2.04 | 0.90 | 1.31 | 2.66 |
| 483 | 0.75 | 0.82 | 1.28 | 0.87 | 0.75 | 0.95 |
| 663 | 0.62 | 1.01 | 0.99 | 0.79 | 1.01 | 0.40 |
| 843 | 0.40 | 1.47 | 0.47 | 0.78 | 1.49 | 0.35 |
| 1023 | 0.27 | 1.79 | 0.41 | 0.58 | 1.90 | 0.45 |

Fig. 7 Friction coefficient of Nimonic 80A and Nimonic 90 versus sliding distance

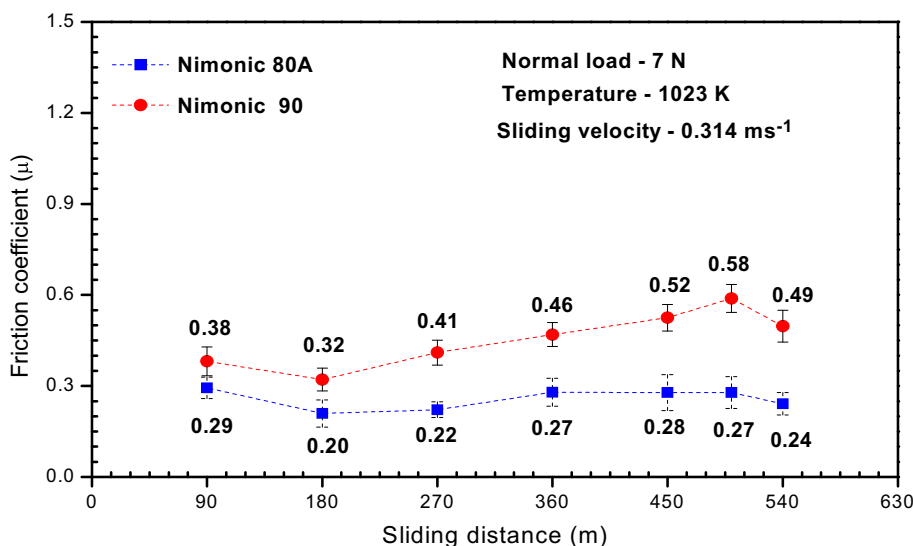
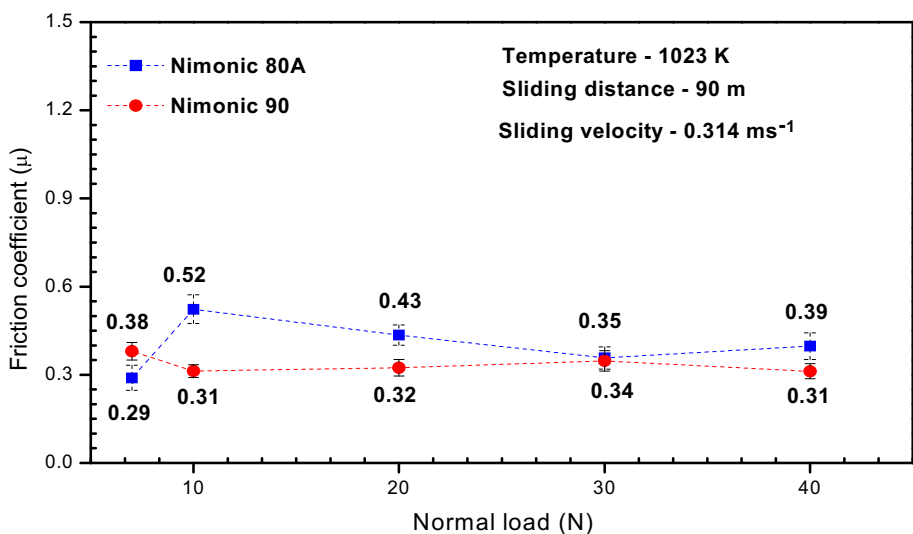


Fig. 8 Friction coefficient of Nimonic 80A and Nimonic 90 versus load



2.3 Experimental Apparatus

All the tribological tests were conducted on ‘pin-on-disc adjustment’ using a high-precision universal tribometer set-up as shown in Fig. 2a. Lower disc specimen of N 80A and N 90 samples rotates, whereas the upper pin specimen of N 75 is fixed for experimental work as shown in Fig. 2b. Inside view of the disc specimen at high temperatures after the sliding test is shown in Fig. 2c. Sliding tests were conducted to study the influence of temperature (T), sliding distance (m) and normal load (F_N) on friction and wear behaviour of N 80A and N 90 alloys. Test parameters adopted for sliding tests are shown in Table 3. The parameters which are held fixed during test excursions are

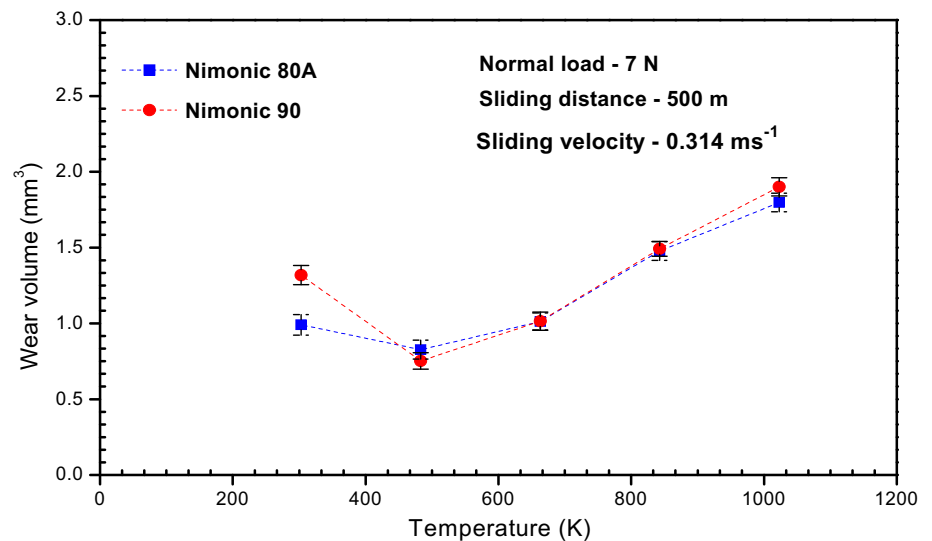
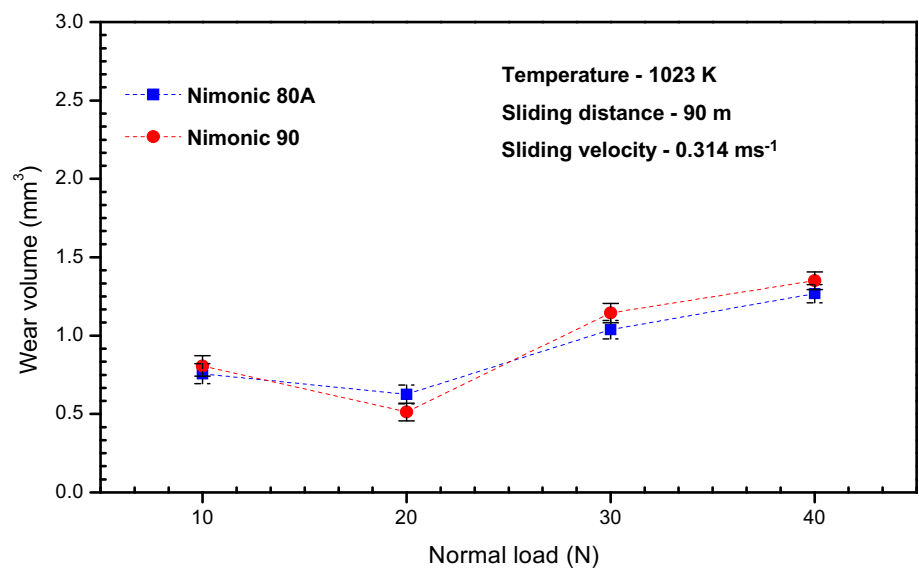
Table 5 Friction coefficient of samples and counterface versus sliding distance

| Element | Sliding distance (m) | | | | | |
|--|----------------------|------|------|------|------|------|
| | 90 | 180 | 270 | 360 | 450 | 540 |
| <i>Friction coefficient (μ)</i> | | | | | | |
| N 80A | 0.29 | 0.20 | 0.22 | 0.27 | 0.27 | 0.24 |
| N 90 | 0.38 | 0.32 | 0.41 | 0.46 | 0.52 | 0.49 |

shown in Table 3. The influence of magnetic field of resistance heating on the metallic wear is not studied in this paper. A minimum of three tests (one test per sample) were conducted for each sliding test condition for better

Table 6 Total wear volume of samples versus sliding distance

| Tribo-pairs | Disc wear volume (mm ³) | Pin wear volume loss (mm ³) |
|-------------|-------------------------------------|---|
| N 80A/N 75 | 1.85 | 0.47 |
| N 90/N 75 | 2.07 | 0.52 |

Fig. 9 Disc wear volume of Nimonic 80A and Nimonic 90 versus temperature**Fig. 10** Disc wear volume of Nimonic 80A and Nimonic 90 versus load

statistical accuracy. Each pin sample and counterface disc was weighed using high-accuracy microbalance before and after each sliding test. Mean weight loss was calculated and this was recorded as a positive value. Before the tests, the sample and counterface were cleaned in an ultrasonic bath with acetone for 15 min. Then, the samples were dried in a

hot air oven for 10 min. After the test, the process was repeated to clean the sample and counterface. The microstructure of the wear track (samples and counterface) was characterized at microscale level using optical microscopy, scanning electron microscope (SEM), equipped with energy-dispersive X-ray spectroscopy [EDS (data

Table 7 Friction coefficient and wear volume loss of samples and counterface versus load

| Load (N) | N 80A against N 75 | | | N 90 against Nimonic N 75 | | |
|----------|--------------------------------|------------------------------------|--|--------------------------------|---|--|
| | Friction coefficient (μ) | Disc wear volume (mm^3) | Pin wear volume loss (mm^3) | Friction coefficient (μ) | Disc wear volume loss (mm^3) | Pin wear volume loss (mm^3) |
| 10 | 0.52 | 0.75 | 0.36 | 0.31 | 0.80 | 0.31 |
| 20 | 0.43 | 0.62 | 0.12 | 0.32 | 0.51 | 0.20 |
| 30 | 0.35 | 1.03 | 0.03 | 0.34 | 1.14 | 0.03 |
| 40 | 0.39 | 1.26 | 0.09 | 0.31 | 1.35 | 0.10 |

Fig. 11 Wear volume of counterface pin Nimonic 75 versus temperature

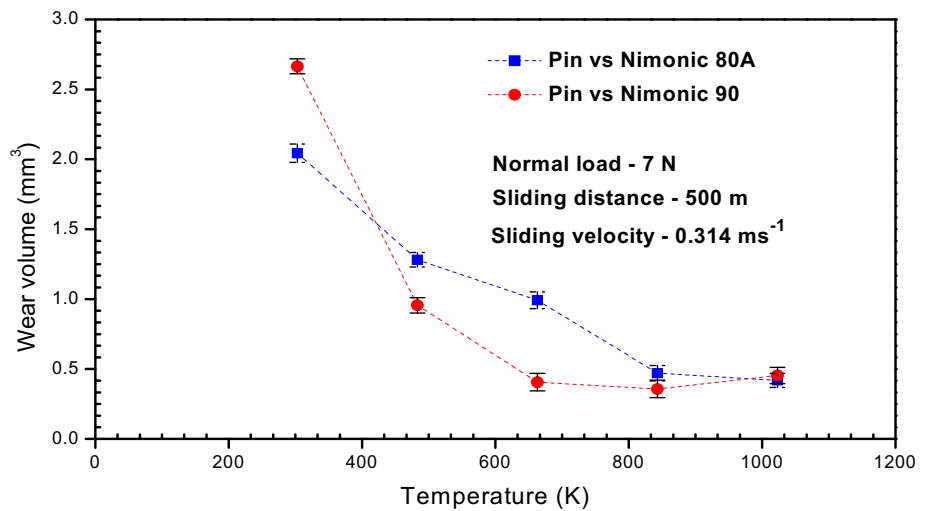
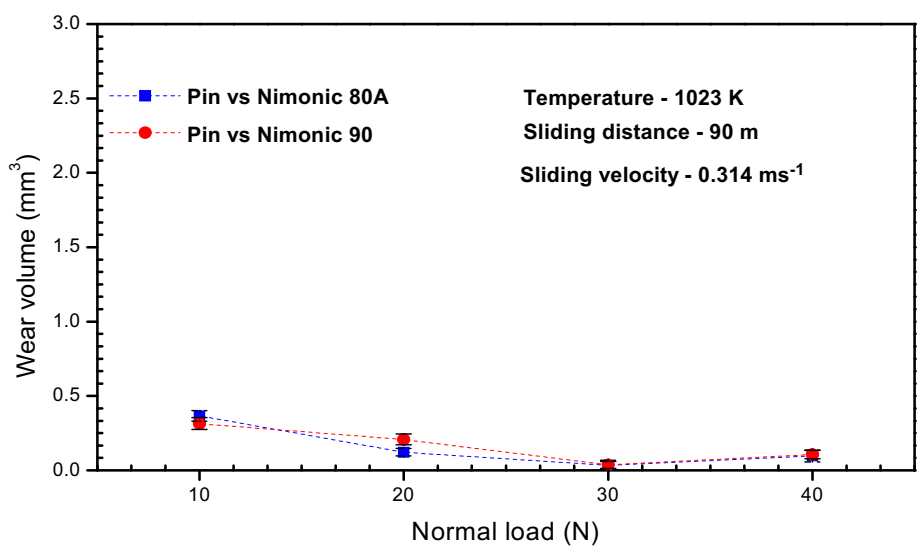


Fig. 12 Wear volume of counterface pin Nimonic 75 versus load



in wt%)), Raman spectroscopy and 3D profilometer to understand the wear mechanism. Wear volume of the pin sample and counterface disc is calculated using Eq. (2) [30] as:

$$\text{Wear volume loss (mm}^3\text{)} = \frac{\text{Weight loss (g)}}{\text{Density of material (g/cm}^3\text{)}} \tag{2}$$

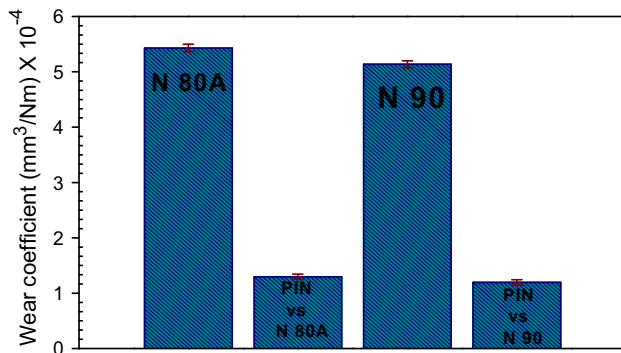


Fig. 13 Wear coefficient of Nimonic 80A and Nimonic 90 against Nimonic 75

The wear coefficient (K_w) was determined by the ratio of the wear volume lost (mm^3) to sliding distance (m) and per unit applied normal load (F_N) and is represented in Eq. (3) [30] as:

$$K_w = \frac{W}{F_N \cdot s} \quad (3)$$

where K_w is the wear coefficient, W is wear volume (mm^3), F_N is the applied load (N) and s is the sliding distance (m).

3 Results and Discussion

The following aspects have been studied during tests, and its results (microhardness, friction coefficient and wear volume) obtained from these studies are shown in following sections.

3.1 Vickers Microhardness (HV)

The variations of HV versus indentation load at different dwell times are shown in Figs. 3 and 4 for N 80A and N 90. It is evident from Figs. 3 and 4 that the values of HV decrease with the increase in indentation load at different dwell times. As the indentation load increases, material undergoes plastic deformation which results in the decrease in the values of HV. Figure 5 shows optical micrographs of indent impression at different indentation loads and dwell times for N 80A alloy. The diagonal values of indentation size/impression increase with the increase in indentation load which results in the decrease in HV values. This phenomenon is known as normal indentation size effect. The plastic deformation of material was observed under higher indentation load of 1000 g and above as shown in Fig. 5. Therefore, the values of HV decrease with the increase in indentation load. The variation of HV with respect to dwell time exhibits that HV values show very slight variation with respect to dwell time. The diagonal values of indentation size remain

constant with respect to dwell time as shown in Fig. 5. Therefore, the values of HV remain constant with the increase in dwell time. The average HV values obtained for N 80A, N 90 and N 75 at 50-g indentation load and 10-s dwell time are 5.13 ± 0.02 , 5.02 ± 0.04 and 5.21 ± 0.07 GPa, respectively.

3.2 Friction Coefficient (μ)

The values of μ versus temperature of N 80A and N 90 against N 75 are shown in Fig. 6. It is evident from Fig. 6 that the value of μ decreases with the increase in temperature. Similar behaviour of μ in the case of different tribo-pairs has also been reported [23]. Highest μ of 0.94 was attained at RT, and lowest μ of 0.27 was obtained at 1023 K in case of N 80A as shown in Table 4, whereas in case of N 90, highest μ of 0.90 was attained at RT and lowest μ of 0.58 was obtained at 1023 K as shown in Table 4. Lowest value of μ was obtained in case of N 80A in comparison with N 90. A clear downward trend in the value μ was observed with the increase in temperature. The decrease in μ with the increase in temperature is attributed to the formation of oxides at higher temperatures. This is called as glazed layer. The presence of glazed layer is confirmed with the help of EDS analysis of both tribo-pairs as shown in Figs. 18, 19, 20, 21, 22, 23, 24 and 25. Results obtained in this research study are in conformity with the results obtained by the researchers [16, 17]. The values of μ versus sliding distance of N 80A and N 90 against N 75 at 1023 K are shown in Fig. 7 (Table 5). At the initial running in period (up to 90 m), the value of μ observed is high as the direct contact between two mating surfaces takes place. After the initial running in period, the value of μ decreases (up to 180 m). The decrease in μ is attributed to the formation of mixed mechanical layer (MML) at the interface. The composition of MML is between compositions of two mating materials and wears debris. This MML is soft and hence the value of μ decreases. After covering the sliding distance of 180 m, composite layer (CL) starts forming. The CL is hard and brittle in nature, and hence, the value of μ starts increasing. Once the CL is completely formed at the interface, the μ attains a steady-state value. The mechanism of formation of MML and CL and their influence on the value of μ is also illustrated in [23]. The values of μ versus load of N 80A and N 90 against N 75 at 1023 K are shown in Fig. 8. It is evident from Fig. 8 that the value μ first increases and then decreases with the increase in applied load in the case of N 80A/N 75 tribo-pair (as given in Table 7). Similar behaviour of μ was also observed in the research study conducted by Pauschitz et al. [23], whereas the value of μ slightly increases with

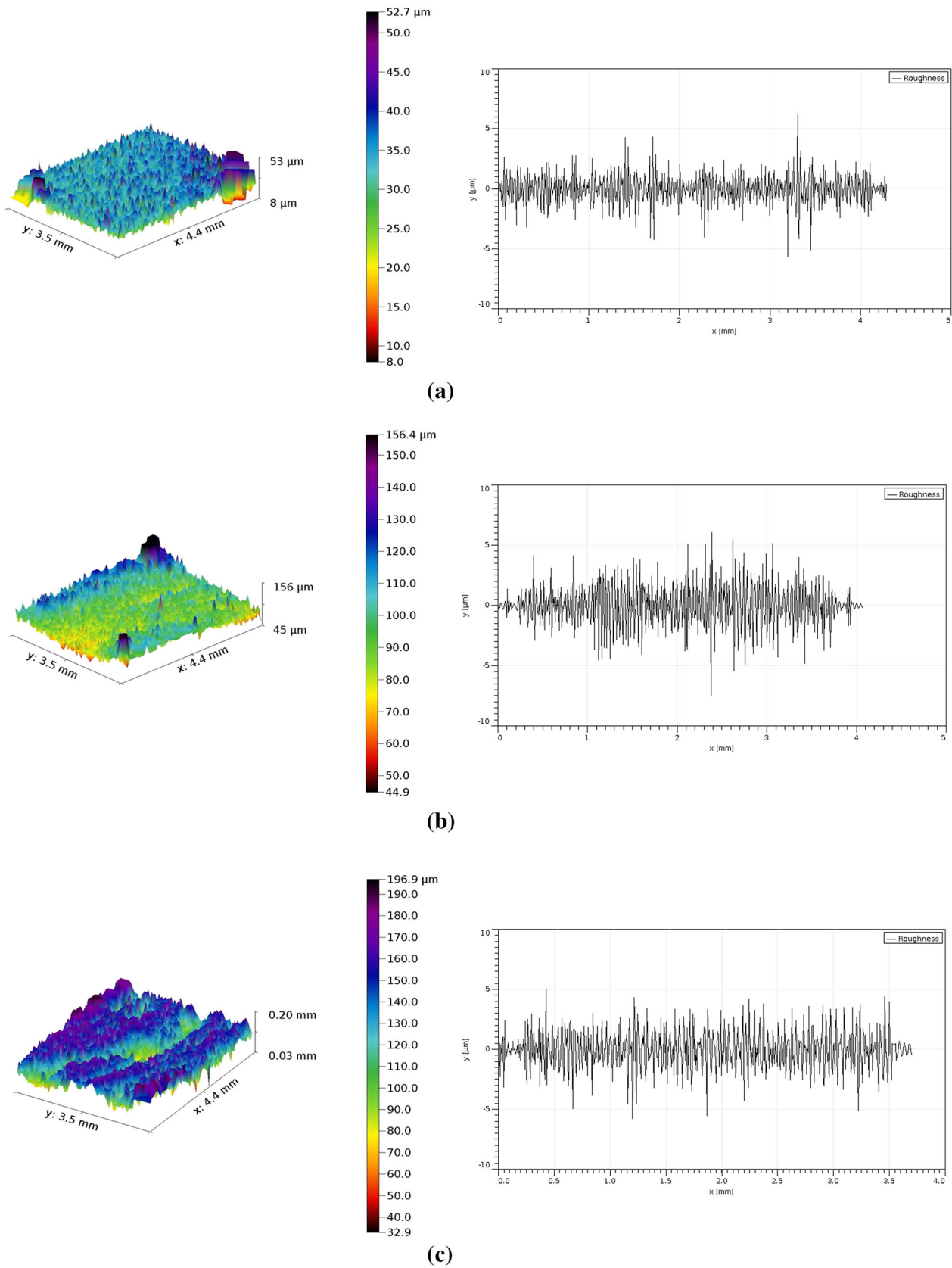


Fig. 14 3D profilometer and roughness images of disc N 80A at different temperatures. **a** RT, **b** 663 K and **c** 1023 K

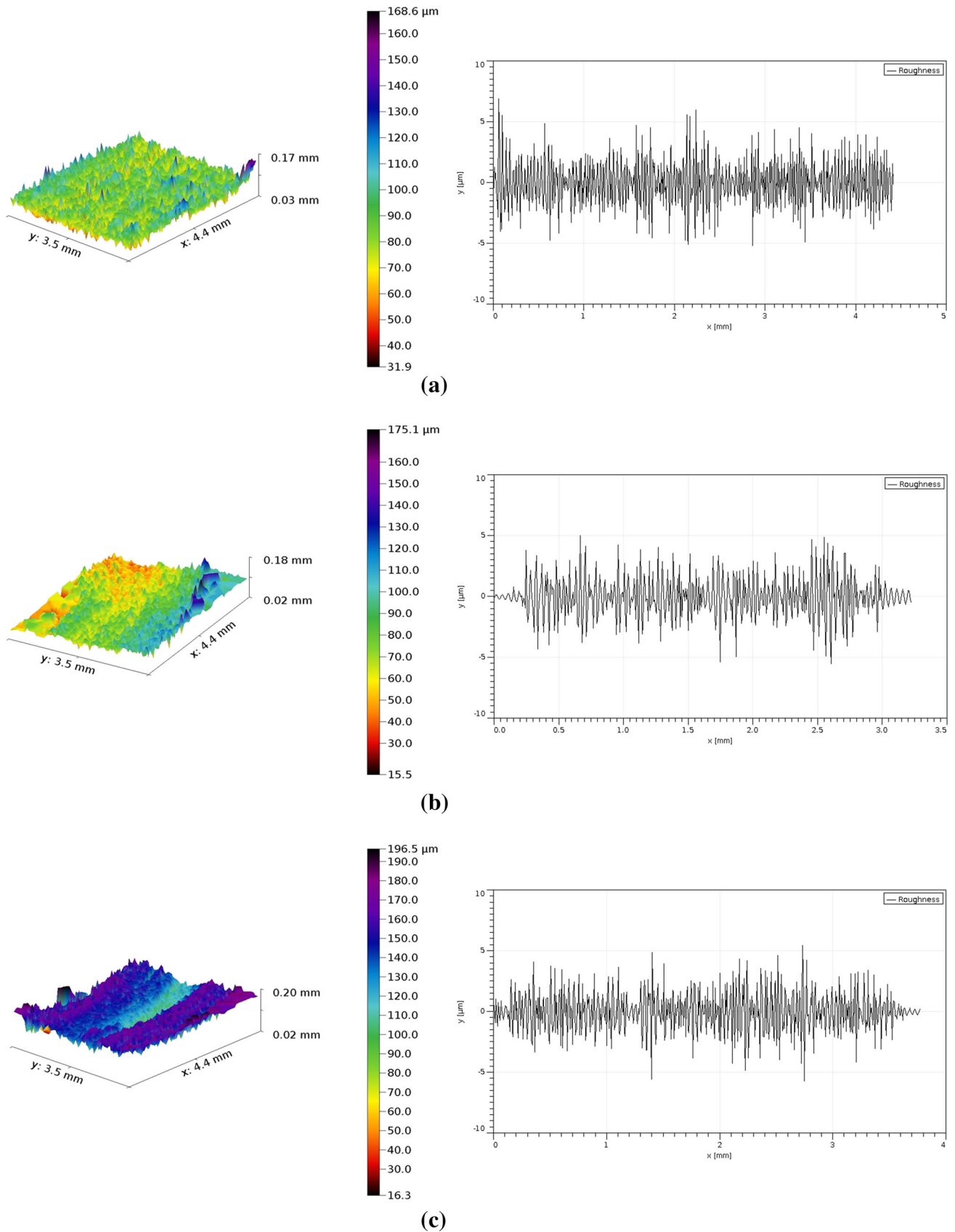


Fig. 15 3D profilometer and roughness images of disc N 90 at different temperatures. **a** RT, **b** 663 K and **c** 1023 K

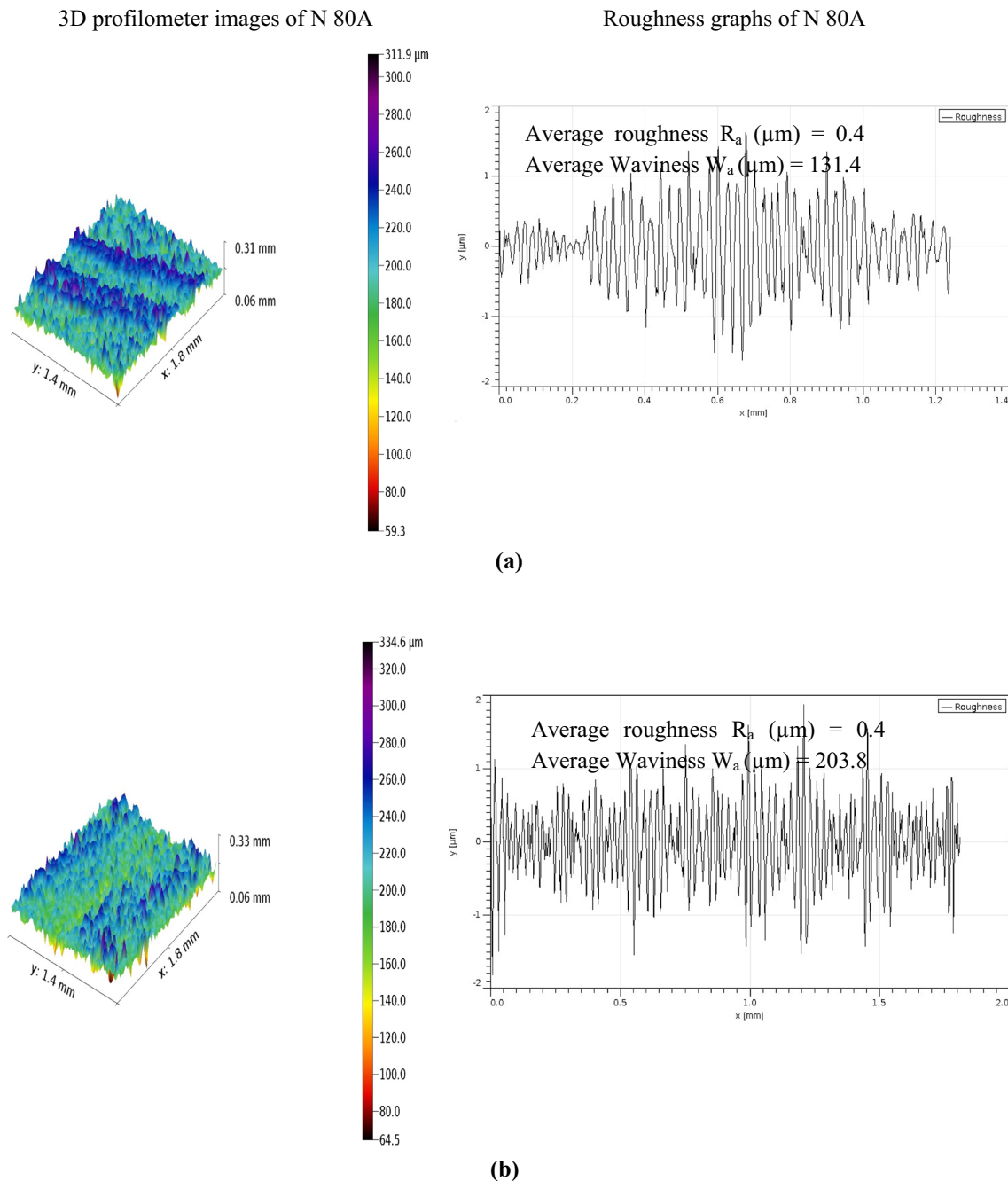


Fig. 16 3D profilometer and roughness images of disc N 80A at load **a** 10 N and **b** 40 N

increases in load in case of N 90/N 75 tribo-pair (as given in Table 7).

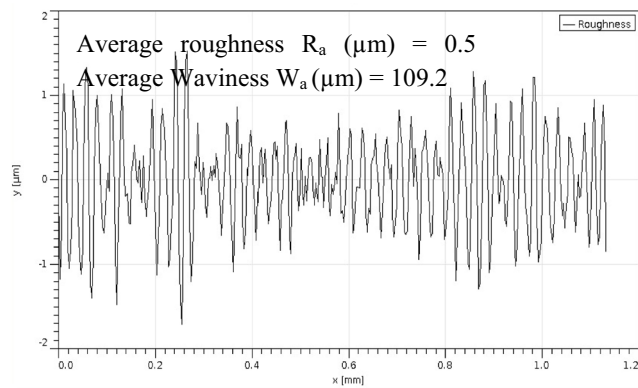
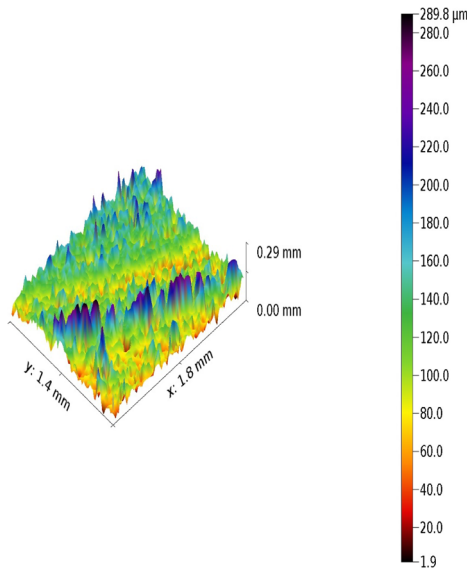
3.3 Wear Behaviour

The calculated cumulative disc wear volume (mm^3) of N 80A and N 90 against N 75 tribo-pairs versus temperature and normal load are shown in Figs. 9 and 10, respectively. The total wear volume of samples after sliding distance test

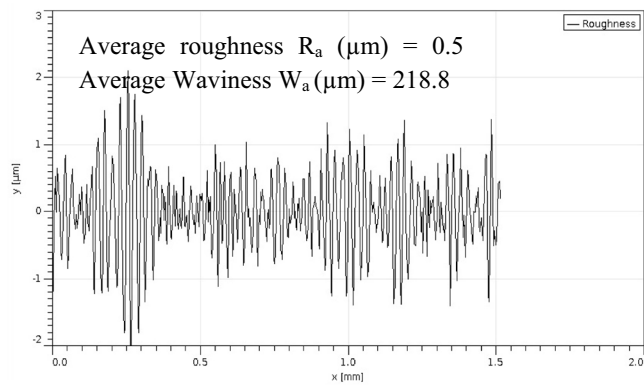
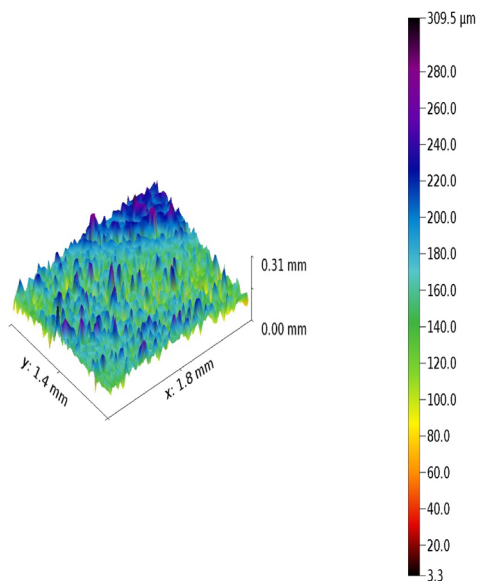
is shown in Table 6. It is evident from Fig. 9 that wear volume of N 80A and N 90 continuously increases with the increase in temperature. Similar, behaviour of wear has also been reported for various other tribo-pairs in [23]. At higher temperature ≥ 843 K, wear volume increases at a slow pace as compared to the increase in the wear at lower temperatures as shown in Table 4. Weight loss was recorded as positive value for all temperature tests. The minimum weight loss of (0.0067 g in N 80A and 0.0061 g

3D profilometer images of N 90

Roughness graphs of N 90



(a)



(b)

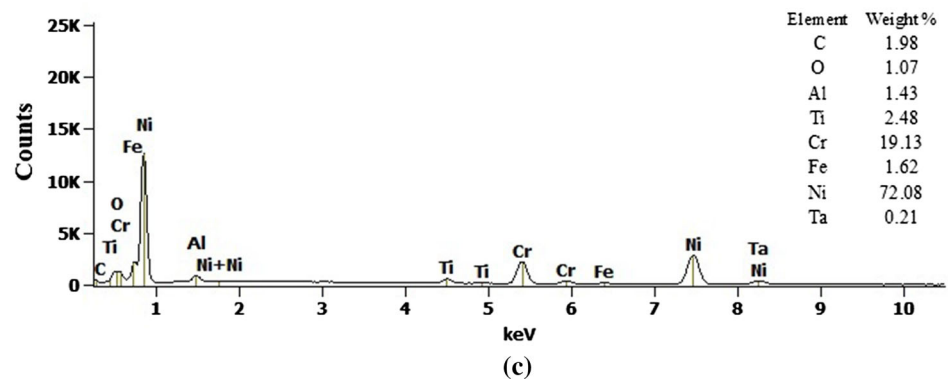
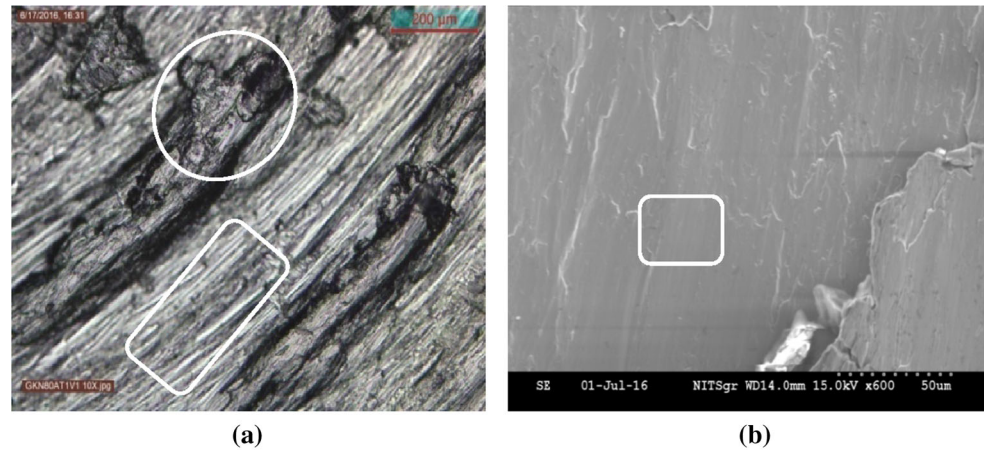
Fig. 17 3D profilometer and roughness images of disc N 90 at load a 10 N and b 40 N

Table 8 Average roughness (Ra) and average waviness (Wa) values of samples versus temperature

| Temperature (K) | N 80A against N 75 | | N 90 against N 75 | |
|-----------------|----------------------|----------------------|----------------------|----------------------|
| | Ra (μm) | Wa (μm) | Ra (μm) | Wa (μm) |
| RT | 0.92 ± 0.60 | 31.05 ± 4.71 | 1.2 ± 0.27 | 78.30 ± 5.89 |
| 663 | 1.3 ± 0.18 | 97.50 ± 7.39 | 1.3 ± 0.19 | 93.50 ± 7.54 |
| 1023 | 1.3 ± 0.29 | 120.30 ± 5.90 | 1.3 ± 0.22 | 118.3 ± 8.26 |

Table 9 Average roughness (Ra) and average waviness (Wa) values of samples versus load

| Load (N) | N 80A against N 75 | | N 90 against N 75 | |
|----------|----------------------|----------------------|----------------------|----------------------|
| | Ra (μm) | Wa (μm) | Ra (μm) | Wa (μm) |
| 10 | 0.4 ± 0.17 | 131.40 ± 6.33 | 0.5 ± 0.28 | 109.20 ± 7.12 |
| 40 | 0.4 ± 0.15 | 203.80 ± 9.84 | 0.5 ± 0.13 | 218.80 ± 10.49 |

Fig. 18 a Optical micrograph, b SEM micrograph and c its EDS spectra of disc N 80A at room temperature

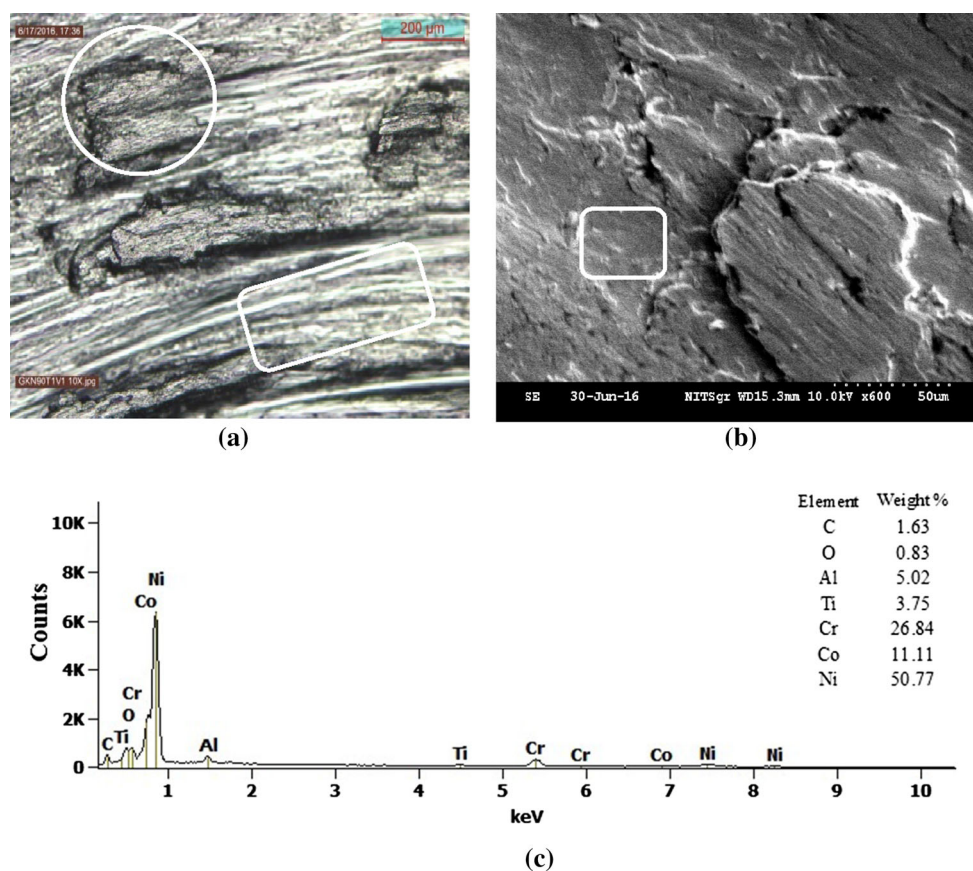
in N 90) was observed at 483 K. It is evident from Fig. 10 and Table 7 that wear volume of N 80A and N 90 continuously increases with the increase in load. The counterface calculated wear volume (mm^3) of N 75 versus temperature and load curves are shown in Figs. 11 and 12. It is evident from Fig. 11 and Table 4 that wear volume of N 75 continuously decreases with the increase in temperature. It is evident from Fig. 12 and Table 7 that calculated wear volume of N 75 decreases with the increase in applied load.

The calculated wear coefficient (K_w) [30] of samples (N 80A and N 90) and counterface (N 75) is shown in Fig. 13. It is evident from Fig. 13 that the calculated K_w value is 5.13×10^{-4} and $5.43 \times 10^{-4} \text{ mm}^3 \text{ N}^{-1} \text{ m}^{-1}$ for N 80A and N 90, respectively. Lower value of K_w means higher wear resistance. N 80A possesses higher wear resistance at higher temperatures, as compared to N 90. N 75 exhibits lowest K_w equal to $1.19 \times 10^{-4} \text{ mm}^3 \text{ N}^{-1} \text{ m}^{-1}$.

3.4 Surface Behaviour

After the experimental studies, wear tracks of N 80A and N 90 were examined under 3D profilometer as shown in Figs. 14, 15, 16 and 17. 3D profilometer was also used to measure the average roughness and average waviness of wear tracks. Average roughness and average waviness are measured in the perpendicular direction to the sliding of wear tracks. Each test was conducted minimum five times for better repeatability. It is evident from Figs. 14 and 15 that 3D profilometer and roughness images are also in agreement with results obtained for N 80A and N 90 at different temperatures. 3D profilometer images of wear track reveals that at room temperature (RT) and average waviness (Wa) of 31.05 and 78.3 μm are obtained in case of N 80A and N 90, respectively. At higher temperature (1023 K), higher average waviness (Wa) of 120.3 and 118.3 μm are obtained in case of N

Fig. 19 a Optical micrograph, b SEM micrograph and c its EDS spectra of disc N 90 at room temperature



80A and N 90, respectively. The average roughness of wear track increases with the increase in temperature up to 663 K and then remains constant as shown in Table 8. It is evident from Figs. 14 and 15 that the values of average waviness continuously increased with the increase in temperature. 3D profilometer and average roughness images of worn surfaces versus load for N 80A and N 90 are shown in Figs. 16 and 17. It is evident from Figs. 16 and 17 that average waviness of the worn surfaces continuously increases with the increase in applied normal load. The lower value of average waviness of 131.4 and 109.2 μm were obtained at 10 N for N 80A and N 90, respectively. The higher value of average waviness obtained at 40 N are 203.8 and 218.8 μm in case of N 80A and N 90, respectively, as shown in Table 9. The average roughness of worn surfaces remains constant with the increase in applied normal load. In the case of applied normal load and temperature, average waviness increase with the increase in wear.

3.5 Study of Wear Mechanism

Surface morphological and elemental analysis of wear tracks were carried out to understand the friction and wear mechanism of N 80A and N 90 against N 75. Wear tracks

of N 80A and N 90 were examined under optical microscope (OM) and SEM. Elemental analysis of wear tracks were carried out using EDS. The results of OM, SEM and EDS are shown in Figs. 18, 19, 20, 21, 22, 23, 24, 25, 26, 27, 28, 29, 30, 31, 32 and 33.

Figures 18a and 19a show wear tracks of N 80A and N 90, respectively. Wear tracks of N 80A and N 90 are covered with patches of material (white circle) and with little grooves on hardened surface (rectangle box) [35]. It is also evident from Figs. 18a and 19a that wear of material is caused due to adhesion; however, higher wear due to adhesion is caused in the case of N 90. Lower wear attained at higher temperature of 663 K (Fig. 9) is attributed to formation of work-hardened metallic layer covering the wear track [35, 36]. This metallic layer protects the wear surfaces and prevents excessive material removal. No oxide layer was present on wear track as confirmed by EDS analysis as shown in Figs. 18c and 19c. EDS analysis area is represented by square box in SEM micrographs. The results obtained from these research studies resemble to the results obtained in [16, 17]. In the absence of formation of oxides, metallic adhesion takes place between two rubbing surfaces. Presence of irregular shape of metallic particles on wear track as shown in Figs. 18b and 19b, indicates that delamination wear mechanism is responsible for wear of

Fig. 20 a Optical micrograph, b SEM micrograph and c its EDS spectra of disc N 80A at 663 K

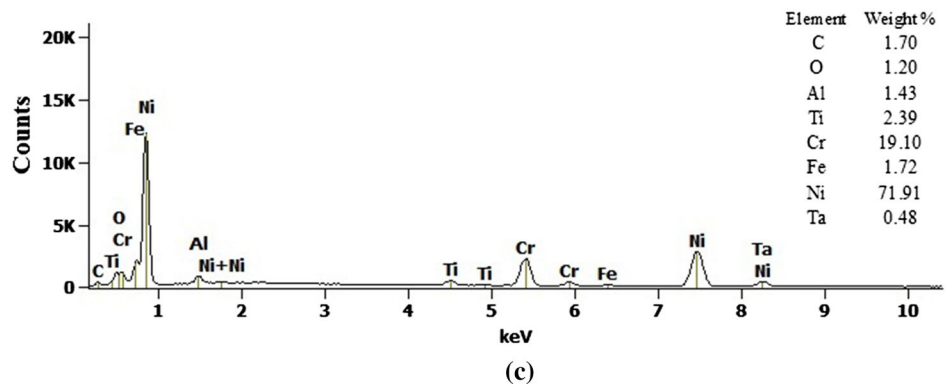
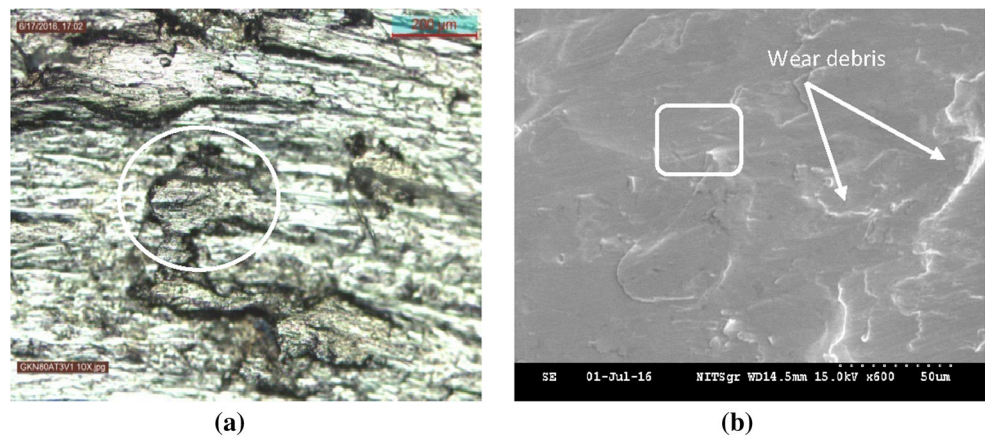


Fig. 21 a Optical micrograph, b SEM micrograph and c its EDS spectra of disc N 90 at 663 K

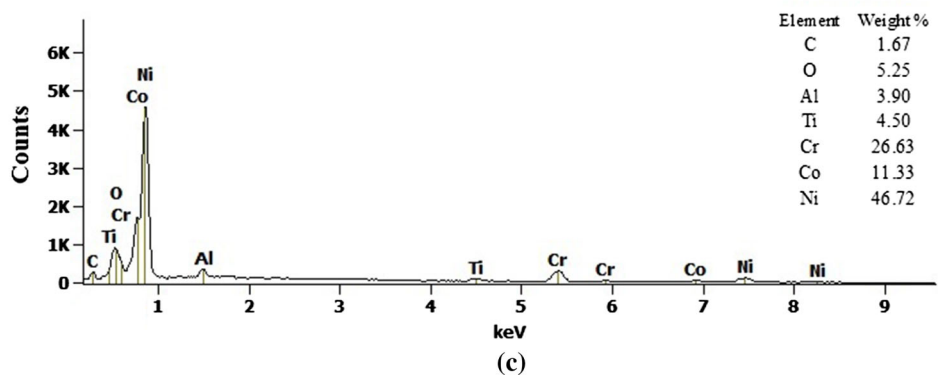
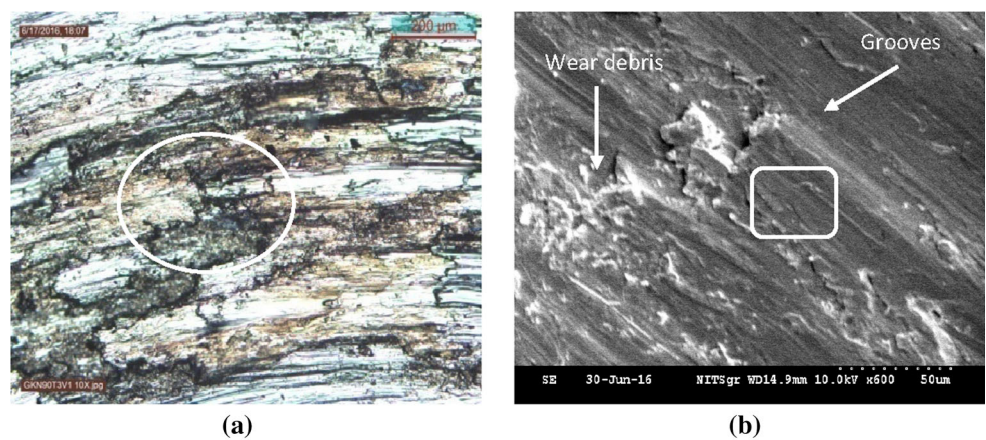


Fig. 22 a Optical micrograph, b SEM micrograph and c its EDS spectra of disc N 80A at 843 K

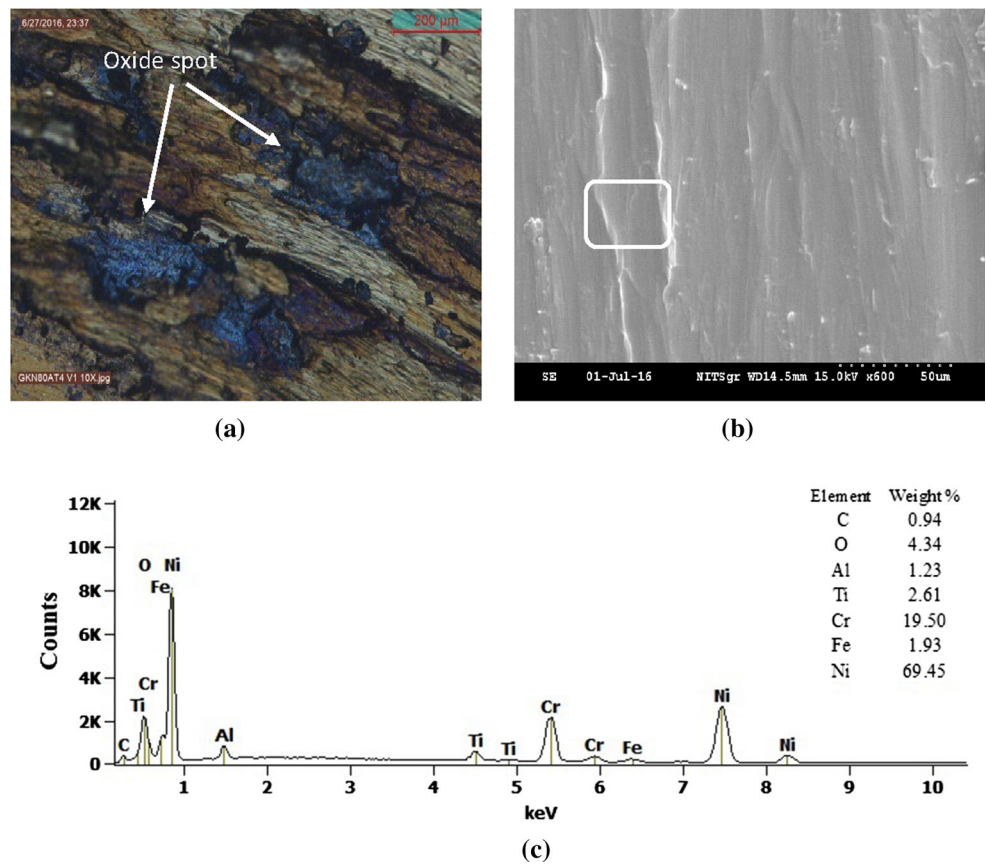


Fig. 23 a Optical micrograph, b SEM micrograph and c its EDS spectra of disc N 90 at 843 K

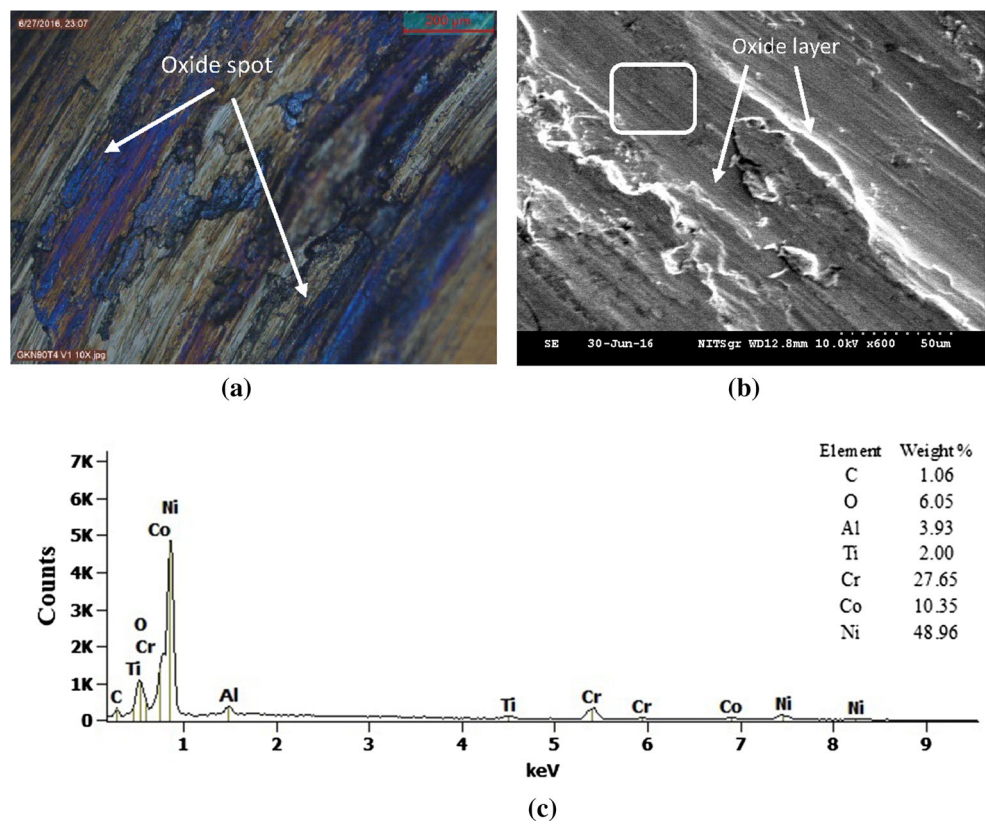
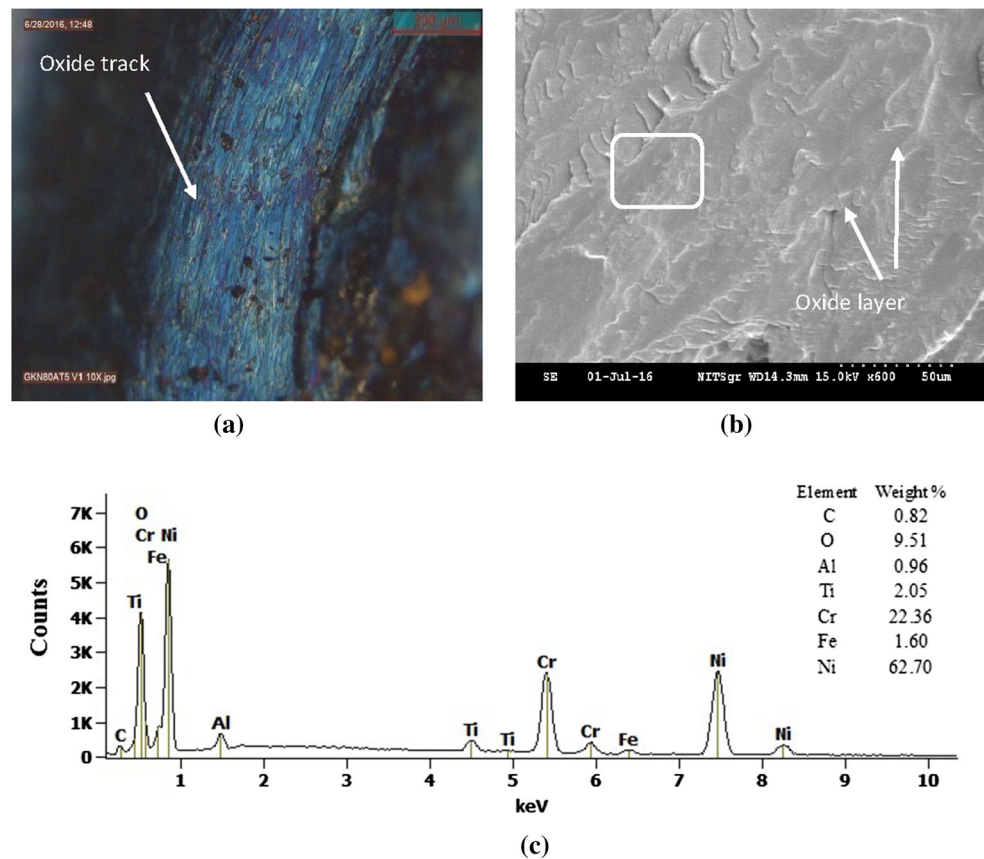


Fig. 24 **a** Optical micrograph, **b** SEM micrograph, and **c** its EDS spectra of disc N 80A at 1023 K



the disc material. Similar wear mechanism is observed for metallic and alloy materials in [24].

With the increase in temperature above 663 K, thermal softening of metallic material takes place at the interface. Similar behaviour of thermal softening of materials above 663 K at the interface has also been reported in [37]. It is evident from Figs. 20a and 21a that a decrease in metallic transfer is observed and only a few patches of transferred material are present on the wear track. The decrease in metallic transfer was accompanied by an increase in the discoloration due to very limited oxidation of exposed metallic surfaces [25]. Metallic discoloration did not mean to build-up wear-protective oxide layers. SEM micrographs (Figs. 20b, 21b) indicate the presence of minor scoring marks and larger flat platelet-like shape on the wear track. EDS analysis confirms the presence of oxide on wear track as shown in Figs. 20c and 21c. It is evident from Figs. 22 and 23 that trace of glaze layer formation and mild wear was first observed at high temperature of 843 K. SEM micrographs observed flat, large metallic irregular shape of oxide debris on wear track as shown in Figs. 22b and 23b. This fine oxide debris is produced by enhanced oxidation of contacting N 80A/N 75 and N 90/N 75 tribo-pairs surfaces. The presence of oxide debris is also

observed in EDS as shown in Figs. 22c and 23c. The oxide layer is developed at high temperatures due to the oxidation of wear debris at the interface. The characteristic of this layer is high hardness and wear resistance [35, 36]. This oxide layer reduces metallic transfer from pin to counterface (disc) at the interface [26]. Formation of oxide layer at the interface of higher temperature reduces wear, as compared to wear at room temperature [27, 28]. It is evident from Figs. 24 and 25 that the surface layers became more compressive with increasing the sliding temperature up to 1023 K; arrest in increasing weight loss at 1023 K was observed in Fig. 9. At higher temperature of 1023 K, presence of compact oxide surface layer decreases. Similar behaviour of compact oxide layer is observed in [16, 17, 19, 27, 28]. This compact oxide surface layer is known as glaze layer. The development of these 'glaze' layers also prevents any loose oxide acting abrasively against the underlying metal. It is evident from Figs. 24b and 25b that SEM micrographs reveal the presence of glaze layer, deformed substrate and glaze/substrate interface. The responsible mechanism for the generation of wear-protective glaze layer involved deformation of surface, intermixing of debris generated from the samples and counterface surfaces, oxidation, welding, further mixing, repeated welding and fracture.

Fig. 25 **a** Optical micrograph, **b** SEM micrograph and **c** its EDS spectra of disc N 90 at 1023 K

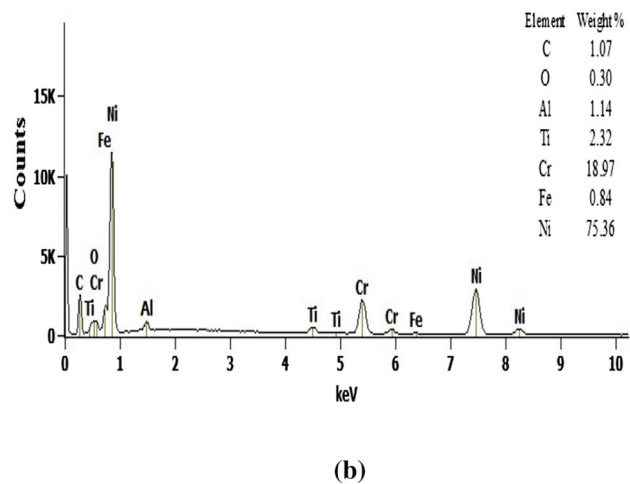
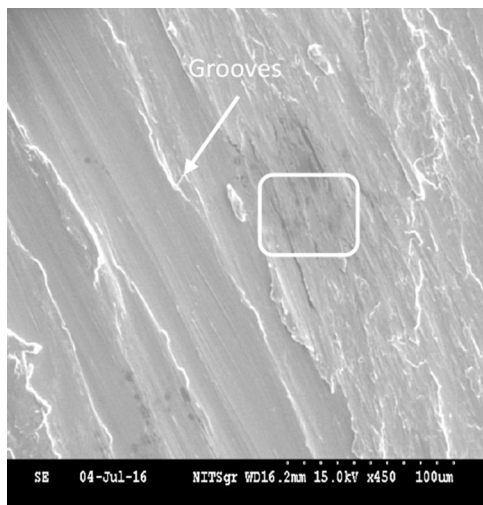
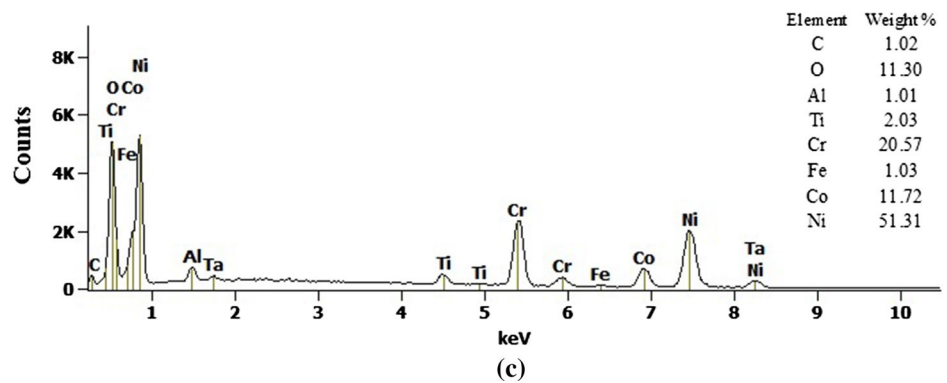
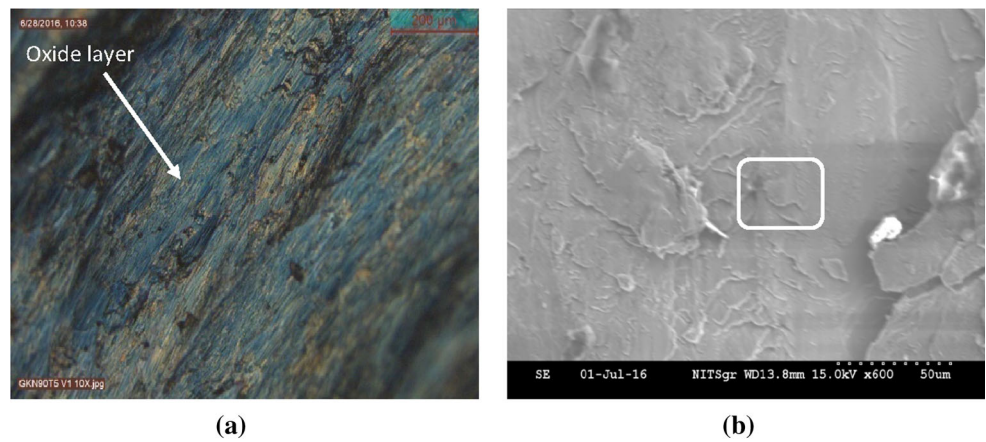


Fig. 26 **a** SEM micrograph and **b** its EDS spectra of counterface N 75 against N 80A at room temperature

This mechanism is aided by high-temperature oxidation and diffusion. The oxide layers on wear track of samples and counterface are deformed and dislocated, which leads to formation of subgrains [23, 38]. These subgrains are then refined with increasing mis-orientation giving

nanostructured grains with angle boundaries (known as fragmentation) [16, 17].

Grooved profiles are observed on worn surfaces of wear track at all temperatures up to 1023 K for counterfaces as shown in Figs. 26, 27, 28, 29, 30, 31, 32 and

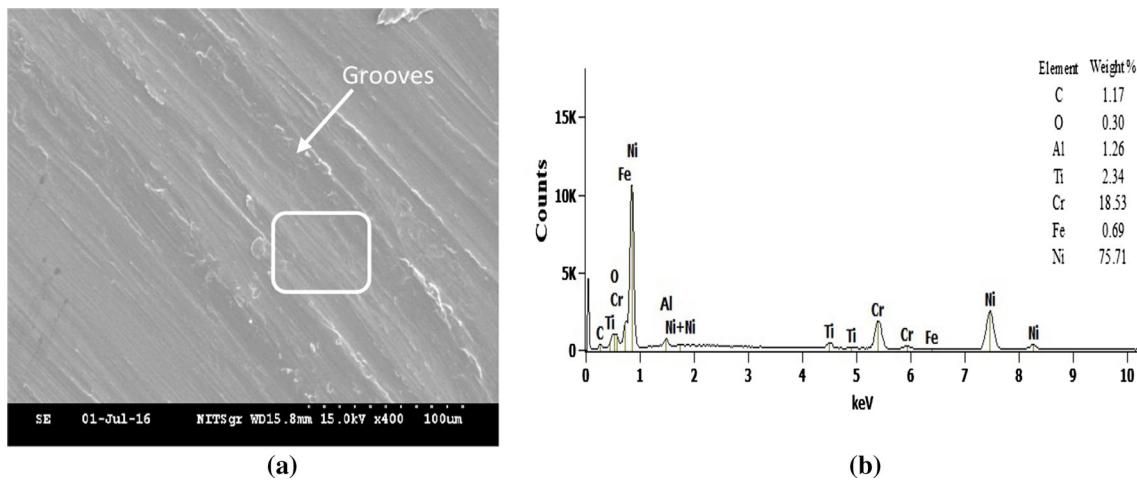


Fig. 27 a SEM micrograph and b its EDS spectra of counterface N 75 against N 90 at room temperature

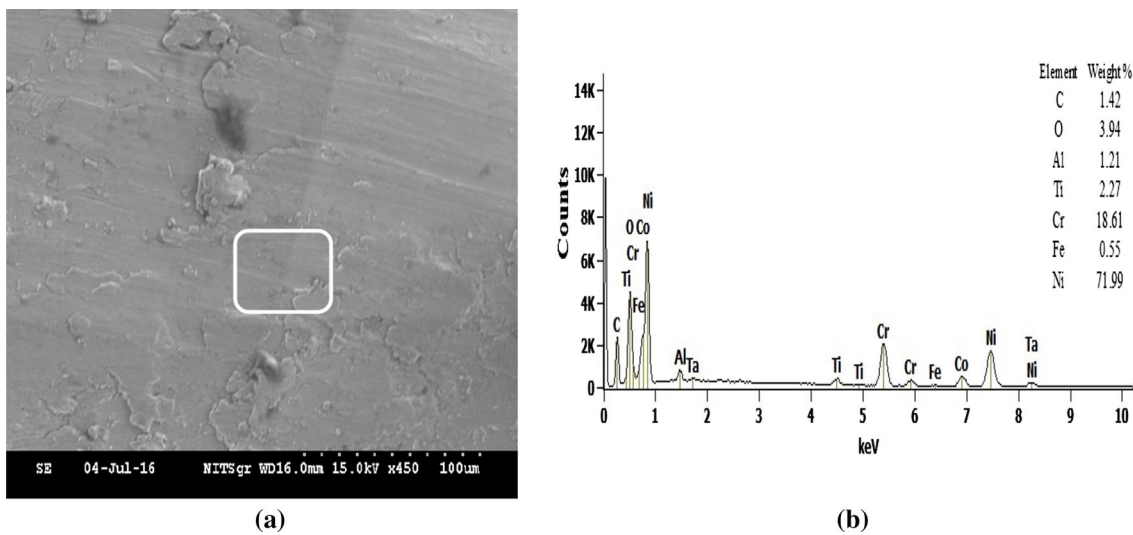


Fig. 28 a SEM micrograph and b its EDS spectra of counterface N 75 against N 80A at 663 K

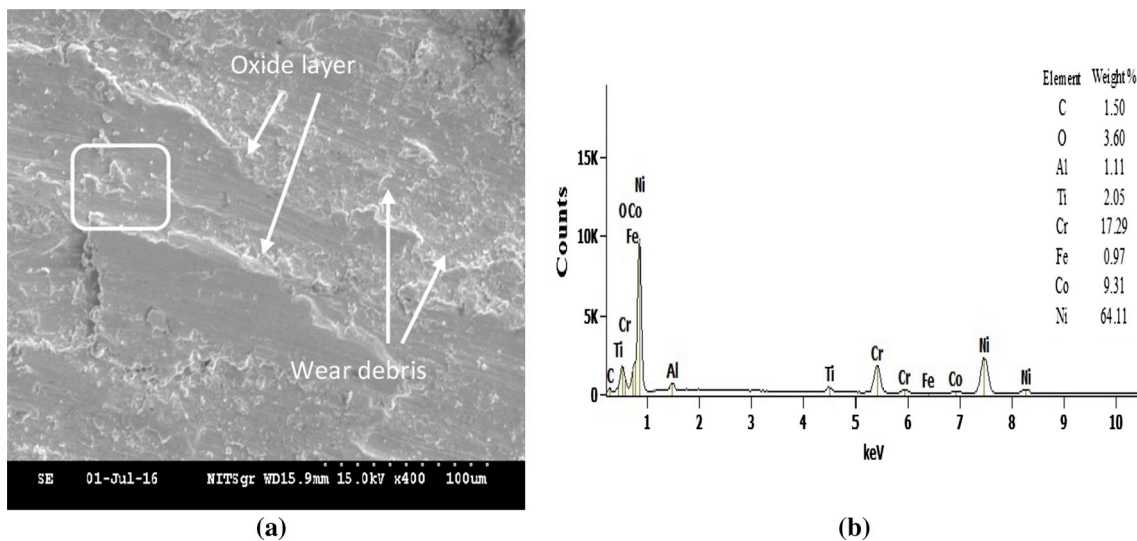


Fig. 29 a SEM micrograph and b its EDS spectra of counterface N 75 against N 90 at 663 K

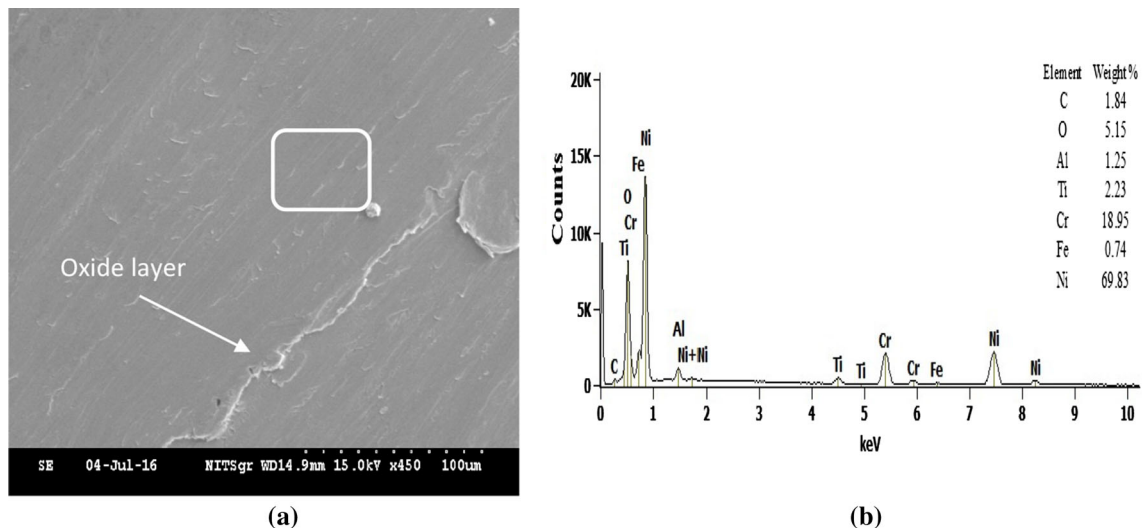


Fig. 30 a SEM micrograph and b its EDS spectra of counterface N 75 against N 80A at 843 K

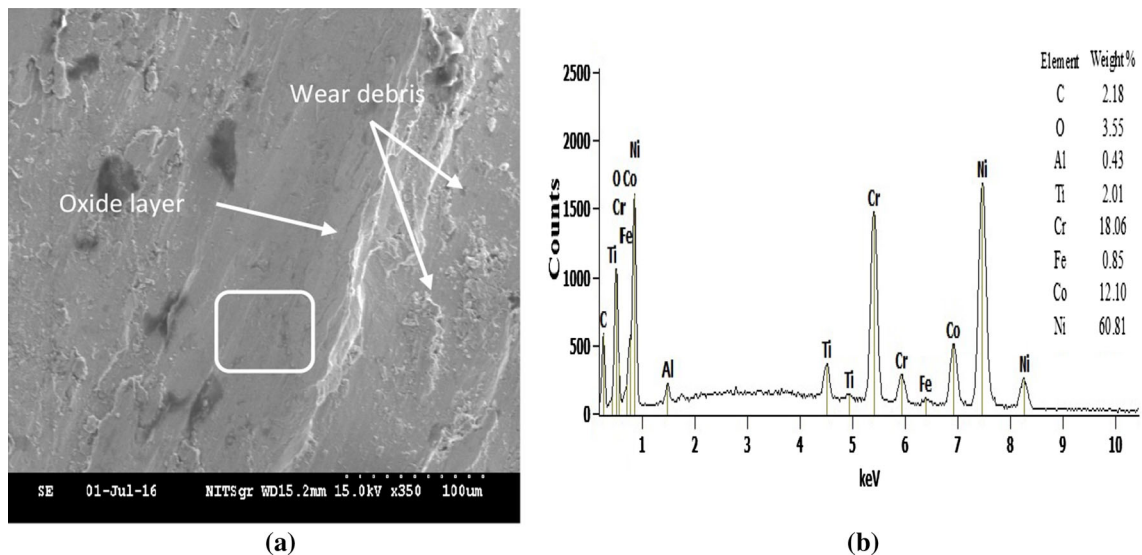


Fig. 31 a SEM micrograph and b its EDS spectra of counterface N 75 against N 90 at 843 K

33, respectively. It is evident from Figs. 26a, 27a that SEM micrographs indicate high metallic transfer due to high wear loss as shown in Fig. 11. This transfer layer develops due to removal and readhesion of metallic material. With the increase in temperature, the level of oxygen increased as confirmed by EDS (square box) and forms oxide layer. It is evident from Figs. 28a and 29a that SEM micrographs indicate that high wear with limited transfer layer development and back-transfer of metallic material to and from samples. Discoloration of worn surfaces of wear track due to limited oxidation at 663 K coincided with reduced transfer layer development and decrease in wear loss as shown in Fig. 11.

Some metallic material re-adheres to the counterface inside the wear track to form asperities; these asperities can only have been created by back-transfer and their quantity increasing with temperature. As the only areas to come into contact with the sample transfer layers are the asperities, it is the peaks of these to which later 'glaze layer' formation is restricted [16, 17]. As the transfer layers underlying the 'glaze layer' on the sample are mixed composition, the only possible source of such composition oxide is the counterface. The asperities must form later in the sliding process when counterface can no longer transfer to the samples (i.e. when increasing oxidation in the transfer layer inhibits further

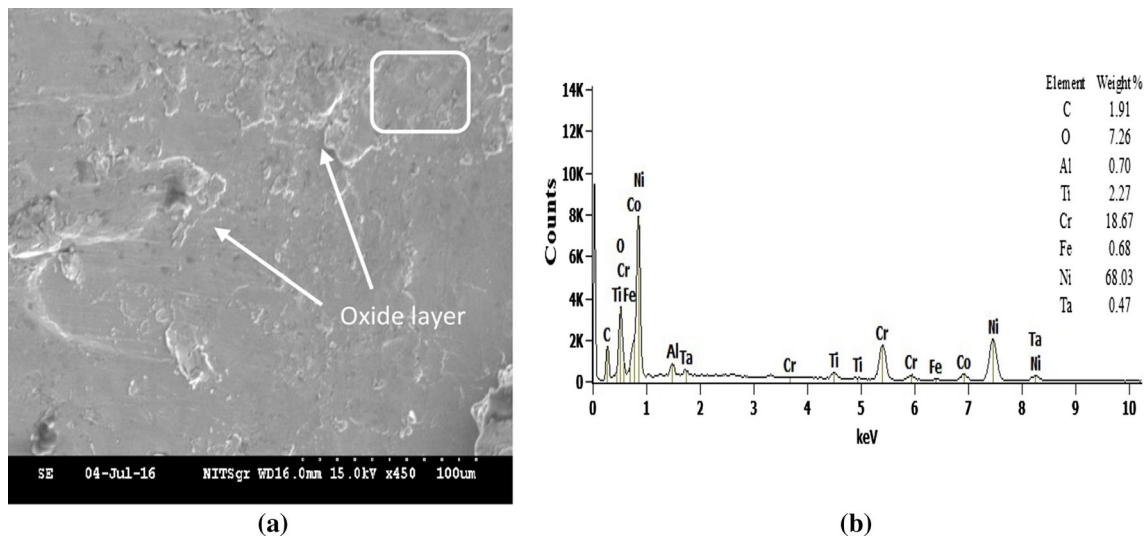


Fig. 32 a SEM micrograph and b its EDS spectra of counterface N 75 against N 80A at 1023 K

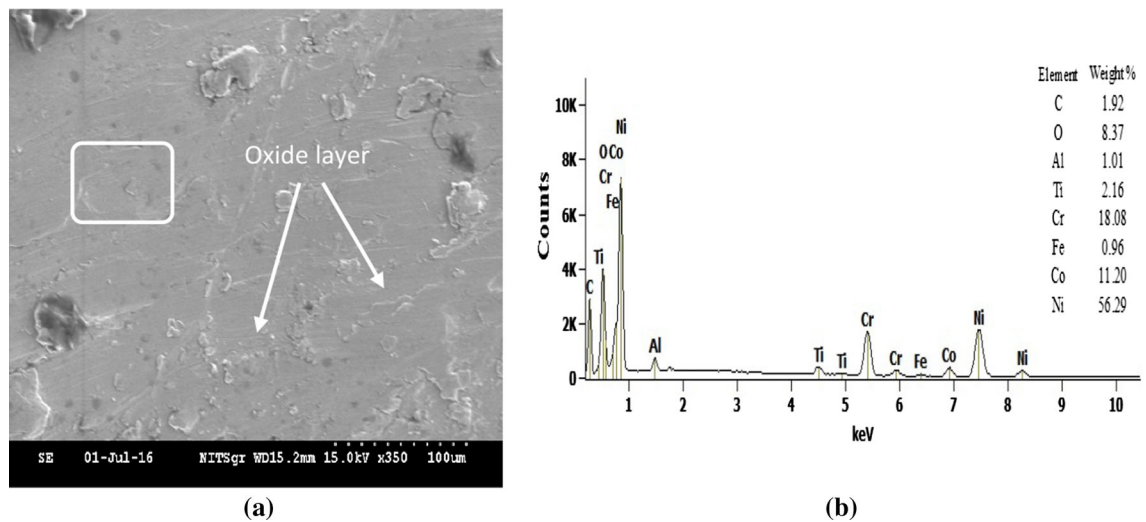


Fig. 33 a SEM micrograph and b its EDS spectra of counterface N 75 against N 90 at 1023 K

metallic layer adhesion), thus favouring back-transfer. Glaze' formation must only begin after back-transfer has created the counterface asperities, and they have begun to interact with the highly oxidized layer on samples transfer layer surface [16, 17]. Trace of glaze formed on the counterface at ≥ 843 K, matching 'glaze' forming temperatures on the samples. This 'glaze' formation was accompanied by large quantities of easily dislodged loose oxide layer appearing within the counterface wear track as shown in Figs. 30a, 31, 32 and 33a. With the increase in temperature, glaze layer cover entered area of wear track and reduces the wear loss as shown in Fig. 11.

3.6 Oxide Composition on Glaze Formation

The presence of compact oxide layer decreases the effect of wear, and this compact oxide layer is in micron (μm) [35–38]. The level of oxide layer produces in metallic debris at higher temperature above 843 K. No oxide layer was present among the metallic debris at RT and 483 K. It is evident from Figs. 34 and 35 that there is the presence of oxide layer on the interface of contacting surfaces of both tribo-pairs at applied load of 7 N, sliding distance of 500 m and at higher temperature (1023 K). The laser Raman spectrometer (inVia Raman, Renishaw plc UK) verified these oxide layers at the sample interface of N 80A, N 90

Fig. 34 Raman image of N 80A and N 90 sample against N 75

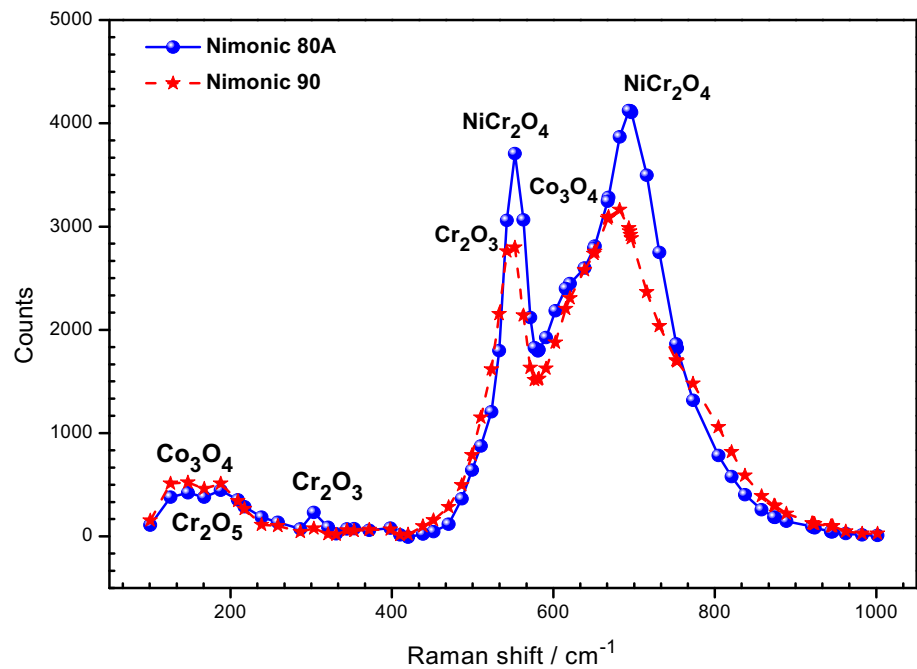
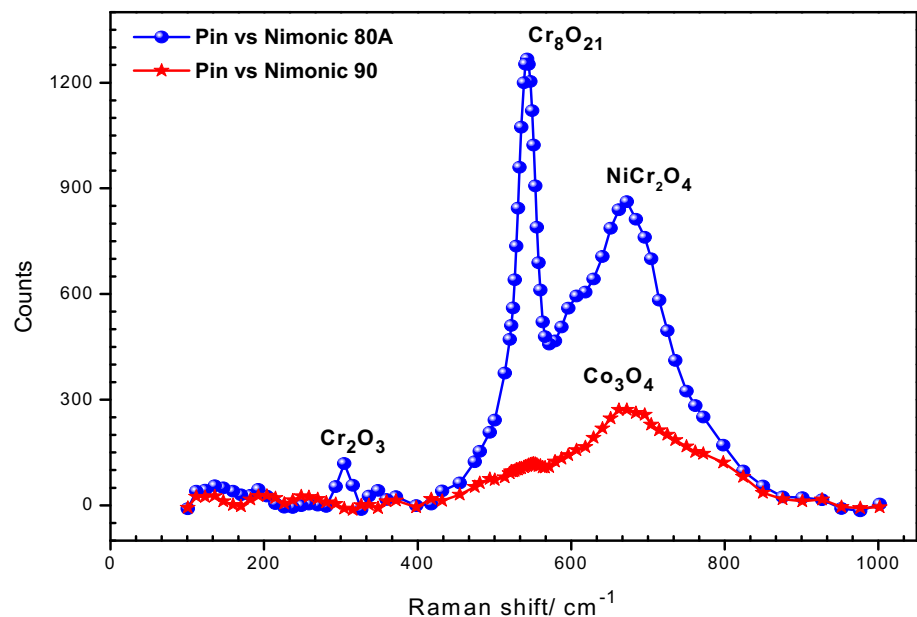


Fig. 35 Raman image of counterface pin N 75 against N 80A and N 90



and N 75 (counterface). The spectrum is acquired using a green laser with a microscope-focused beam of 532 nm wavelength and 80-s exposure time. CCD array detector is used. NiCr_2O_4 [34] shows doublets are presented at Raman bands of 552 and 687 cm^{-1} , Cr_2O_3 [32] at Raman bands of 305 cm^{-1} and Cr_2O_5 [32] at Raman bands of 188 cm^{-1} in case of N 80A, whereas Cr_2O_3 [31] at Raman bands of 550 cm^{-1} , Co_3O_4 [33] at Raman bands of 678 and 191 cm^{-1} in case of N 90 as shown in Fig. 34. It is evident from Fig. 35 that at the interface of counterface against both alloys the oxide layers are presented. Cr_8O_{21} [32] at

Raman band of 549 cm^{-1} , NiCr_2O_4 [31] at Raman band of 687 cm^{-1} and Cr_2O_3 [32] at Raman bands of 305 cm^{-1} are presented in case of N 80A counterface, whereas Co_3O_4 [34] at Raman band of 675 cm^{-1} are presented in case of N 90 counterface. The strong/dominant peaks of Raman bands of NiCr_2O_4 oxide nichromate phase are shown in case of N 80A, whereas Co_3O_4 and Cr_2O_3 peaks are present in case of N 90. The oxide layers slow down the effect of friction and wear at higher temperatures; these oxides are heat resistant and are used as chemical agent at higher temperatures, etc.

4 Conclusions

In the present study, we investigated the friction and wear behaviour of N 80A and N 90 against N 75 superalloys between at RT and 1023 K. The major conclusions from the study can be summarized as follows:

- The wear volume loss of the Ni-based pin at 1023 K is approximately five times lower compared to wear at RT in case of N 80A and six times in case N 90. This can be attributed to the formation of protective oxide layers, referred to as glaze layers. At 1023 K, protective oxide layers almost completely suppress the direct metal-to-metal contact. This was confirmed by SEM, EDS and Raman spectroscopy of pin and samples (disc) wear surfaces.
- A standard severe wear regime was observed at RT and 483 K, which results in formation of work-hardened transfer layer on the samples (disc) and reducing wear. With the increase in temperature, the oxidation inhibits metallic transfer. At ≥ 663 K, no work-hardened transfer layer was observed, which results in samples wear increase. A mixed metal oxide transfer layer forms on the wear track of samples at this temperature, later overlaid by wear-resistant glaze layer. Glaze formation reduces affect of wear on both samples and counterface at higher temperatures.
- Average roughness of wear track increases with increases in temperature up to 663 K. Further, with the increase in temperature, surface roughness remains constant. The average waviness of wear track increases with the increase in temperature and load.
- The tribo-pair N 80A/N 75 exhibits good results as compare to N 90/N 75 tribo-pair. N 80A possesses high wear resistance as compare to N 90.

References

1. Sun, W., Qin, X., Guo, J., Lou, Zhou, L.: Microstructure stability and mechanical properties of a new low cost hot-corrosion resistant Ni–Fe–Cr based super alloy during long-term thermal exposure. *Mater. Des.* **69**, 70–80 (2015)
2. Liu, J.K., Cao, J., Lin, X.T., Song, X.G., Feng, J.C.: Microstructure and mechanical properties of diffusion bonded single crystal to polycrystalline Ni-based super alloys joint. *Mater. Des.* **49**, 622–626 (2013)
3. Betteridge, W.: *The Nimonic Alloys*, pp. 72–93. Arnold, London (1959)
4. Srinivasan, N., Prasad, Y.V.R.K.: Hot working charctersitics of Nimonic 75, 80A and 90 super alloys: a comparsion using processing maps. *J. Mater. Process. Technol.* **51**, 171–192 (1995)
5. Rynio, C., Hattendorf, H., Klower, J., Eggeler, G.: On the physical nature of tribo-layers and wear debris after sliding wear in a super alloy/steel tribo system at 25 and 573 K. *Wear* **317**, 26–38 (2014)
6. Nimonic 80A datasheet: Publication number SMC-099. Copyright & Special Metals Corporation. www.specialmetals.com (2004)
7. Gill, S.P.A., McColvin, G., Strang, A.: Stress relaxation of nickel-based super alloy helical springs at high temperatures. *Mater. Sci. Eng. A* **613**, 117–129 (2014)
8. Nimonic 90 datasheet: Publication number SMC-080. Copyright & Special Metals Corporation. www.specialmetals.com (2004)
9. Khakian, M., Nategh, S., Mirdamadi, S.: Effect of bonding time on the microstructure and isothermal solidification completion during transient liquid phase bonding of dissimilar nickel-based superalloys IN738LC and Nimonic 75. *J. Alloys Compd.* **653**, 386–394 (2015)
10. Nimonic 75 datasheet: Publication number SMC-058. Copyright & Special Metals Corporation. www.specialmetals.com (2004)
11. Lewis, R., Dwyer-Joyce, R.S., Josey, G.: Investigation of wear mechanisms occurring in passenger car diesel engine inlet valves and seat inserts. SAE (Paper 1999-01-1216) (1999)
12. Lewis, R., Dwyer-Joyce, R.S.: *Automotive Engine Valve Recession*. Wiley, London (2002)
13. Stott, F.H., Lin, D.S., Wood, G.C.: The structure and mechanism of formation of the glaze oxide layers produced on nickel-based alloys during wear at high temperatures. *Corros. Sci.* **13**, 449–469 (1973)
14. Gee, M.G., Jennett, N.M.: High resolution characterisation of tribochemical films on alumina. *Wear* **193**, 133–145 (1995)
15. Wood, P.D., Datta, P.K., Burnell-Gray, J.S., Wood, N.: Investigation into the high temperature wear properties of alloys contacting against different counterfaces. *Mater. Sci. Forum* **251**(254), 467–474 (1997)
16. Inman, I.A., Rose, S.R., Datta, P.K.: Studies of high temperature sliding wear of metallic dissimilar interfaces II: Incoloy MA956 versus Stellite 6. *Tribol. Intl.* **39**, 1361–1375 (2006)
17. Inman, I.A., Datta, P.K., Du, H.L., Burnell-Gray, J.S., Pierzgal-ski, S., Luo, Q.: Studies of high temperature sliding wear of metallic dissimilar interfaces. *Tribol. Int.* **38**, 812–823 (2005)
18. Birol, Y.: High temperature sliding wear behavior of Inconel 617 and Stellite 6 alloys. *Wear* **269**, 664–671 (2010)
19. Lancaster, J.K.: The formation of surface films at the transition between mild and severe metallic wear. *Proc. R. Soc. Lond. A* **273**, 466–483 (1962)
20. Welsh, N.C.: The dry wear of steels 2, interpretation and special features. *Philos. Trans. R. Soc.* **257A**, 51–70 (1965)
21. Welsh, N.C.: The dry wear of steels 1, the general pattern of behavior. *Philos. Trans. R. Soc.* **257A**, 31–50 (1965)
22. Pauschitz, A., Roy, M., Franek, F.: On the chemical composition of layers formed during sliding of metallic alloys at high temperature. *Tribol. Int.* **188**, 127 (2003)
23. Pauschitz, A., Roy, M., Franek, F.: Mechanisms of sliding wear of metals and alloys at elevated temperatures. *Tribol. Int.* **41**, 584–602 (2008)
24. Suh, N.P.: The delamination theory of wear. *Wear* **25**, 111–124 (1973)
25. Jiang, J., Stott, F.H., Stack, M.M.: The effect of partial pressure of oxygen on the tribological behavior of a nickel-based alloy N80A at elevated temperatures. *Wear* **203–204**, 615–625 (1997)
26. Li, X.Y., Tandon, K.N.: Micro-structural characterization of mechanically mixed layer and wear debris in sliding wear of an Al alloy and an Al based composite. *Wear* **245**, 148–161 (2000)
27. Mishra, R.S., McFadden, S.X., Mukherjee, A.K.: Tensile super-plasticity in nano-crystalline materials produced by severe plastic deformation. In: Lowe, T.C., Valiev, R.Z. (eds.) *Investigations and Applications of Severe Plastic Deformation*, pp. 231–240. Kluwer, Dordrecht (1994)

28. Ghosh, A.K., Huang, W.: Severe deformation based progress for grain subdivision and resulting microstructures. In: Lowe, T.C., Valiev, R.Z. (eds.) *Investigations and Applications of Severe Plastic Deformation*, pp. 29–36. Kluwer, Dordrecht (2000)
29. Gong, J., Wang, J., Guan, Z.: A comparison between Knoop and Vickers hardness of silicon nitride ceramics. *Mater. Lett.* **56**(6), 941–944 (2002)
30. Henry, S.D.: *Friction, Lubrication and Wear Technology*, vol. 18, p. 478. ASM Handbook, ASM International, Noveltty (1992)
31. Kim, J.H., Hwang, I.S.: Development of an in situ Raman spectroscopic system for surface oxide films on metals and alloys in high temperature water. *Nucl. Eng. Des.* **235**, 1029–1040 (2005)
32. Monnereau, O., Tortet, L., Grigorescua, C.E.A., Savastrua, D., Iordanescua, C.R., Guinneton, F., Notonierb, R., Tonettob, A., Zhangc, T., Mihailescud, I.N., Stanoid, D., Trodahl, H.J.: Chromium oxides mixtures in PLD films investigated by Raman Spectroscopy. *J. Optoelectron. Adv. Mater.* **12**(8), 1752–1758 (2010)
33. Gallant, D., Pezolet, M., Simard, S.: Optical and physical properties of cobalt oxide films electro-generated in bicarbonate aqueous media. *J. Phys. Chem. B.* **110**, 6871–6880 (2006)
34. Rashad, M., Rusing, M., Berth, G., Lischka, K., Pawlis, A.: CuO and Co₃O₄ nano-particles: synthesis, characterizations and Raman Spectroscopy. *J. Nano Mater.* Article ID 714853, 6 (2013)
35. Inman, I.A., Datta, P.S.: Studies of high temperature sliding wear of metallic dissimilar interfaces IV: Nimonic 80A versus Incoloy 800HT. *Tribol. Int.* **44**, 1902–1919 (2011)
36. Inman, I.A., Datta, P.S.: Studies of high temperature sliding wear of metallic dissimilar interfaces III: incoloy MA956 versus Incoloy 800HT. *Tribol. Intl.* **43**, 2051–2071 (2010)
37. Inman, I.A.: *Compacted oxide layer formation under conditions of limited debris retention at the wear interface during high temperature sliding wear of superalloys*. PhD thesis, Northumbria University, UK (2003) published by Dissertation.com (2006)
38. Inman, I.A., Datta, S., Du, H.L., Burnell-Gray, J.S., Luo, Q.: Microscopy of glazed layers formed during high temperature sliding wear at 750 C. *Wear* **254**, 461–467 (2003)